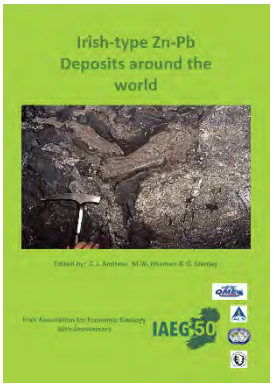

Irish Association for Economic Geology

(founded 1973)

Home Page: https://www.iaeg.ie

Mineralogical and chemical characterization of Mississippi Valley–type mineralization in British Columbia and Alberta, Canada: Implications for ore-forming processes

Daniel J. Kontak[1], Suzanne Paradis[2], Zach Waller[1] & Mostafa Fayek[3]

[1]Harquail School of Earth Sciences, Laurentian University, 935 Ramsey Lake Road, Sudbury, Ontario, Canada P3E 2C6
[2]Geological Survey of Canada, 9860 West Saanich Road, Sidney, British Columbia, Canada V8L 4B2
[3]Department of Geological Sciences, University of Manitoba, Winnipeg, Manitoba, Canada R3T 2N2

Corresponding Author: Daniel J. Kontak dkontak@laurentian.ca

To cite this article: Kontak, D.J., Paradis, S., Waller, Z. & Fayek, M. (2023) Mineralogical and chemical characterization of Mississippi Valley–type mineralization in British Columbia and Alberta, Canada: Implications for ore-forming processes. *In:* Andrew, C.J., Hitzman, M.W. & Stanley, G. '*Irish-type Deposits around the world*', Irish Association for Economic Geology, Dublin. 629-656.
DOI: https://doi.org/10.61153/EVJZ9918

To link to this article: https://doi.org/10.61153/EVJZ9918

Mineralogical and chemical characterization of Mississippi Valley–type mineralization in British Columbia and Alberta, Canada: Implications for ore-forming processes

Daniel J. Kontak[1], Suzanne Paradis[2], Zach Waller[1] & Mostafa Fayek[3]

[1]*Harquail School of Earth Sciences, Laurentian University, 935 Ramsey Lake Road, Sudbury, Ontario, Canada P3E 2C6*
[2]*Geological Survey of Canada, 9860 West Saanich Road, Sidney, British Columbia, Canada V8L 4B2*
[3]*Department of Geological Sciences, University of Manitoba, Winnipeg, Manitoba, Canada R3T 2N2*

Abstract A comprehensive study of samples from MVT–type base-metal (Zn-Pb) deposits from across the Canadian Cordillera was done to compare and contrast features and assess their relevance in the context of sulphide mineralization. Petrography and supported CL imaging indicates early host rock dissolution to form secondary fine-grained dolostone during marine cementation is followed by multiple generations of dolomite cements (low T, fine-grained to coarser, higher T varieties) that overlaps with Zn-Pb sulphides which is succeeded by a later barren calcite stage. Ore-stage dolomite is often rich in Fe (<1.3 wt. % FeO) and hosts small sphalerite inclusions. Sphalerite-hosted fluid inclusions record Th values (77–214°C) and salinities (1–28 wt. % equiv. NaCl±$CaCl_2$) that reflect fluid mixing with no single fluid type related to sulphide mineralization. In situ SIMS $\delta^{18}O_{VSMOW}$ data for dolomite and calcite (13 to 33‰) suggest involvement of several fluids (i.e., seawater, basinal, meteoric) over a large temperature range at varying fluid-rock ratios. *In situ* SIMS $\delta^{34}S_{VCDT}$ data for sphalerite and pyrite indicate a large variation (8 to 33‰), but with smaller ranges (<2 to 3‰) **f**or the settings studied, and suggest reduced S was produced dominantly via TSR processes from homogeneous sulphur reservoirs. Together the datasets suggest involvement of several fluids in the mineralizing process with mixing of a S-poor, metal-bearing fluid with a metal-poor, S-bearing fluid.

Keywords: British Colombia and Alberta, MVT-deposits, mineralogy, mineral textures, fluid inclusions, stable isotopic data.

Introduction

Carbonate-hosted base-metal (i.e., Zn-Pb) deposits of western Canada (i.e., Canadian Cordillera and Western Canadian Sedimentary Basin) are Mississippi Valley–type (MVT) mineral systems. As such, they are epigenetic, stratabound, carbonate-hosted sulphide bodies dominated by Zn and Pb ores (sphalerite, galena) occluding porosity due to dissolution or collapse features (e.g., breccias. The ore settings are generally formed in carbonate platform settings which are now found in relatively undeformed orogenic foreland rocks, but also foreland thrust belts. Their formation is attributed to fluid migration as part of basin evolution, with mineralization due to mixing of low-temperature, oxidized, metalliferous fluids with another fluid(s) that either initiate or provides the H_2S needed to cause sulphide formation at the site of mineralization (Leach *et al*., 2005, 2010a; Wilkinson, 2014).

The MVT deposits of western Canada (Figs. 1, 2) vary in many aspects - age, physical and chemical properties of their host rocks, diverse metals (Zn–Pb±Ag±Cu; see recent summary in Paradis *et al.*, 2023), ore textures, and thermal-chemical features of ore fluids. This diversity of features provided the basis for a review of these deposits as part of a single integrated study to compare and contrast many of their relevant features in order to better address if differences might reflect common or dissimilar mineralizing processes. This work, presented in more detail by Kontak *et al.* (2022) followed on that of previous studies (e.g., Paradis & Nelson, 2007; Paradis *et al*., 2007; Paradis *et al.*, 2015; Paradis & Simandl, 2017; Drage & Paradis, 2018). This work relied on archived materials from previous studies (see above) and followed an in situ fluid-chemical protocol applied to other carbonate settings (Mathieu *et al.*, 2015, 2022; Hahn *et al.*, 2018) that involved detailed petrography using transmitted and reflected light microscopy,

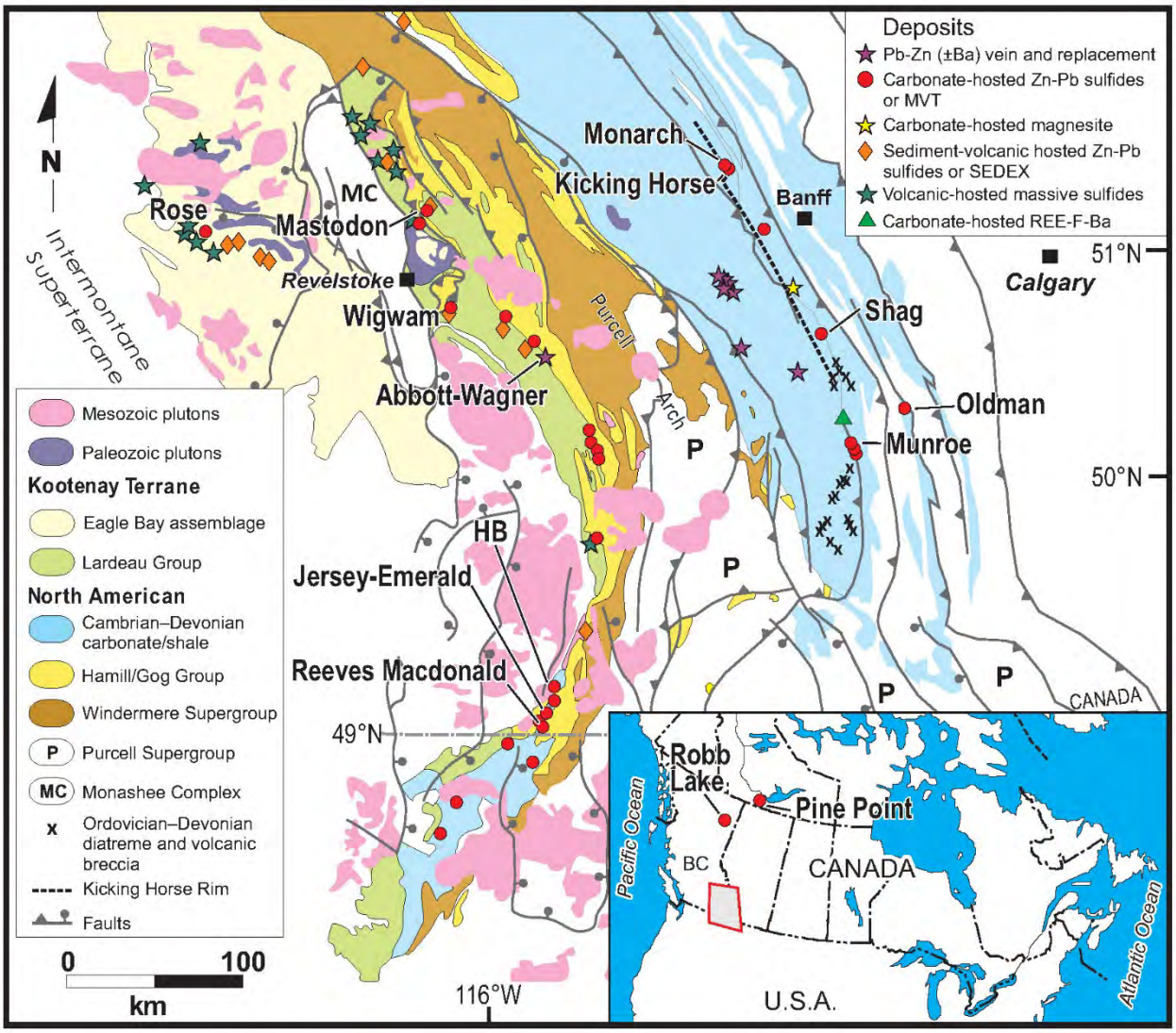

Figure 1: *Regional geological map of southeastern British Columbia (outlined in inset) with locations of the carbonate-hosted Zn-Pb deposits mentioned in the paper. Note the location of the Pine Point and Robb Lake deposits, northern British Columbia and the Northwest Territories, respectively, are shown in in Figure 2. Figure and sources of information from Kontak et al. (2022).*

scanning electron microscopy–energy dispersive spectroscopy (SEM-EDS), and cathodoluminescence (CL) that formed the basis of mineral paragenesis which was then used for subsequent mineral chemical and isotopic (O, S) analysis and fluid inclusion studies. The present contribution is derived from this latter work (see Kontak *et al.*, 2022).

Geological Context of Study Areas

Here are briefly summarized the salient geological information for the deposit settings broken down into geographic areas (Figs. 1, 2) following on extensive earlier studies that determined context of the deposits such as regional geology, dolomitization, and nature of mineralization: 1) the Rocky Mountain Fold and Thrust Belt; 2) the Kootenay Arc; 3) Western Canadian Sedimentary Basin. See Kontak *et al.* (2021) for the relevant bibliography for these areas.

Rocky Mountain Fold and Thrust Belt

This geological domain, part of the North American Cordillera, is a zone (<300 km wide) of east-verging shallow thrust faults and décollement folding coincident with the transition from the Cordilleran miogeocline and the North American Craton; it extends from the Yukon to southeast California (e.g., Price, 1981). In the Canadian Cordillera, stratabound MVT-type Zn-Pb occurrences are hosted in platform carbonate rocks in the Rocky Mountains crossing from British Columbia into Alberta, which are described in two areas below.

In the northern Rocky Mountains, the Robb Lake Zn-Pb deposit (British Columbia) is the largest outcropping and the most extensively explored MVT deposit. It is hosted in Silurian to Devonian dolostone of the Mucho-McConnell Formation; importantly the latter parallels the local trend of the Devonian

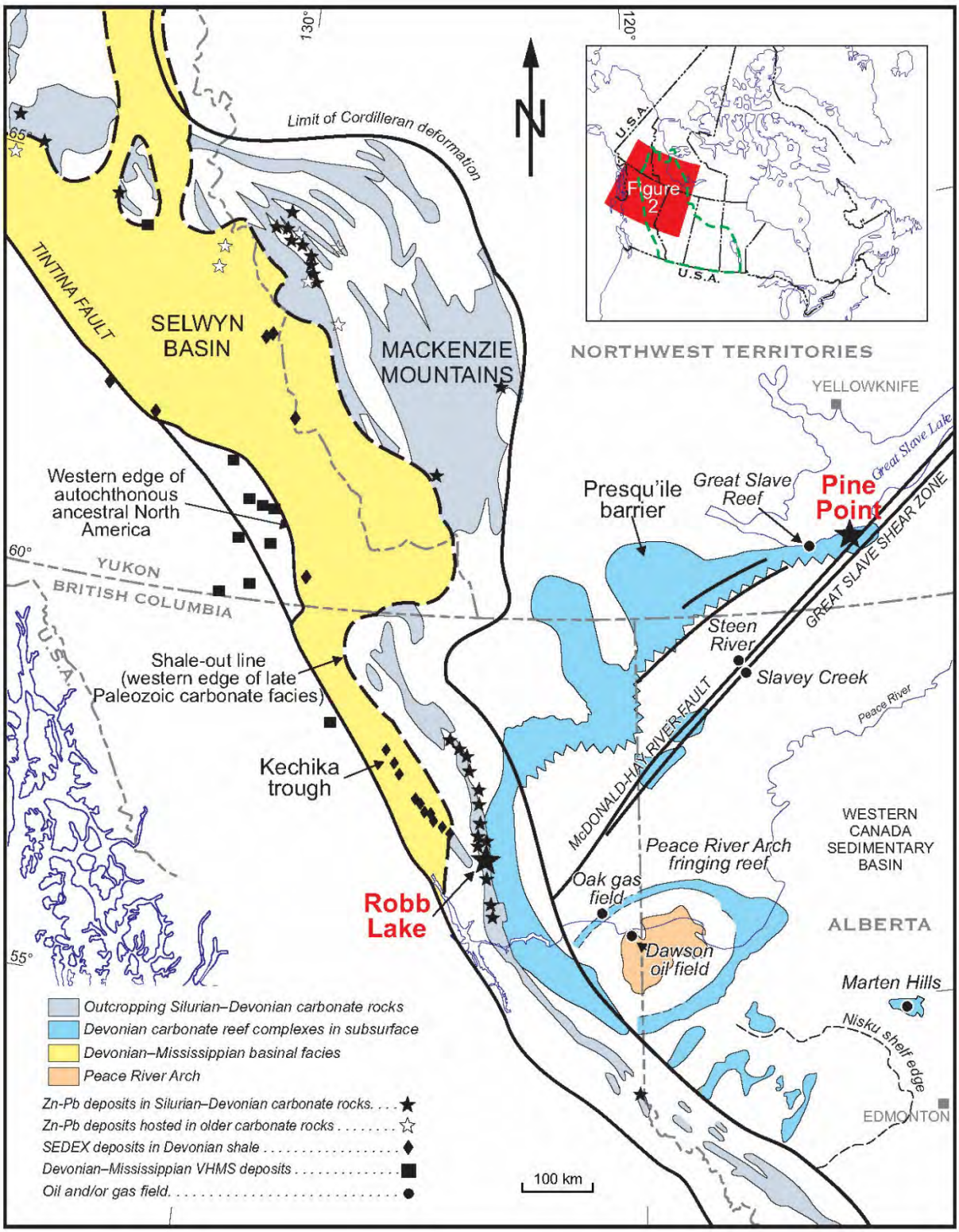

Figure 2: *Location of carbonate-hosted MVT–type Zn-Pb deposits and related areas within the Western Canadian Sedimentary Basin and the northern Rocky Mountain districts mentioned in this paper (i.e., Robb Lake, Pine Point, Robb Lake, Martens Hills, Steen River, Slavey Creek, Dawson oil field, Oak gas field, and Great Slave Reef). Map shows their stratigraphic, structural, and tectonic setting. Also note that locations of sedimentary exhalative (SedEx) and volcanic-hosted massive sulphide (VHMS) deposits along the Devonian shelf margin are shown for reference. Figure and sources of information from Kontak et al. (2022).*

shelf margin that departs from the overall northwest Cordilleran trend and may reflect deep basement structures (Nelson *et al.*, 2002). The deposit consists of numerous stratabound and crosscutting mineralized zones of sphalerite, galena, and pyrite manifest as breccias, veins, and stockworks (Paradis & Nelson, 2007).

In the southern Canadian Rocky Mountains, numerous deposits and prospects, including Kicking Horse, Monarch, Shag, Munroe, and Oldman (Paradis *et a*l., 2020), occur along the southeastern part of the Canadian Cordillera. This area is underlain by platformal carbonate strata, deeper water basinal strata, and minor magmatic arc rocks (McMechan, 2012); additionally, this part of the Rocky Mountains is dominated by thrust faults, almost all of which are east verging (Price, 1981). The mineralization occurs in Cambrian to Devonian carbonate reefs and breccias throughout the belt.

Kootenay Arc

This domain is a large, west-facing, monoclinal feature with an aggregate stratigraphic thickness up to 20 km (Price, 1981). The mineral deposits occur in a 400 km long, north-trending, arcuate structural zone from northeast Washington (U.S.A.) to southern British Columbia (e.g., Höy, 1982). Within this belt are numerous deposits such as Reeves MacDonald (zones at Reeves, MacDonald, O'Donnell, Annex, Point, Prospect, B.L., No. 4, and Red Bird), Jersey-Emerald, HB, Abbott-Wagner, Rose, Wigwam, and Mastodon. The stratabound deposits are hosted in miogeoclinal carbonate rocks of the lower Cambrian Badshot Formation and the Reeves member of the Laib Formation (Paradis, 2007; Simandl *et al.*, 2020) where carbonate rocks are dolomitized, brecciated, and silicified (Paradis, 2007). Intense deformation has modified many of the primary features in these deposits, which has led to different interpretations of their formation, including sedimentary exhalative (SedEx) and syngenetic-diagenetic origins (i.e., Irish-type), as summarized in Paradis (2007) and Paradis *et al.* (2015).

Western Canadian Sedimentary Basin

This vast sedimentary basin, that underlies 1 400 000 km^2 of western Canada, consists of relatively undisturbed middle Proterozoic to lower Tertiary (i.e., Palaeogene) sedimentary successions that thin eastwards (Paradis *et al*., 2006). Deposition occurred in two successive tectono-sedimentary environments: 1) a late Proterozoic to Middle Jurassic passive continental margin; and 2) a Middle Jurassic to Oligocene foreland basin (Price, 1994; Pană, 2006). The MVT mineralization is hosted by Cambrian to Devonian carbonate rocks throughout a large part of this basin in northern Alberta, most notably in the Pine Point district. Below are described two relevant settings.

In northern Alberta the Peace River Arch region (Fig. 2) hosts the most favourable carbonate rocks for MVT mineralization. The sequence onlaps the Precambrian crystalline basement and unmetamorphosed early to mid-Proterozoic clastic rocks of the Athabasca Group, with the overlying sequence having lesser potential (Pană, 2006). Importantly, these favourable rocks are overlain in the east by Quaternary and Neogene strata (<445m) whereas in the west they are buried (<1000m) under post-Devonian rocks. Thus, exposure restricts exploration (and discoveries) to the northeastern portions of the basin. Studied samples are from occurrences in drill core that exhibit MVT-style mineralization in dolostone (Marten Hills, Steen River, and Slavey Creek; see Fig. 2).

The Peace River Arch specifically was a large cratonic uplift that remained topographically elevated until the Middle to Late Devonian. It formed a stable, east-northeast–trending basement structure prior to the deposition of the Middle Devonian carbonate rocks (O'Connell *et al.*, 1990). From this area, samples studied come from the Dawson oilfield and Oak gas field within this arch.

The well- known Pine Point district, comprising around one hundred Zn-Pb deposits of southern Northwest Territories (N.W.T.; Fig. 2) lies between exposed Precambrian Shield to the east and the northern Rocky Mountains to the southwest in Middle Devonian carbonate strata (Pană, 2006). These MVT deposits are hosted in dolomitized carbonate rocks of the Presqu'ile Barrier Reef (Adams *et al.*, 2000; Hannigan, 2006). The reef, 200m thick, >100 km long, and 10 km wide, is mineralized at its northeastern end.

Petrographic Features

Mineralogy

Samples have a mineralogy typical of MVT deposits (e.g., Fig. 3; see Leach & Sangster, 1993; Paradis *et al.*, 2007) with the general abundances of gangue and ore phases summarized in Tables 1 to 3 based on petrographic study of relevant materials. Several carbonate stages (Fig. 3a, b) are noted that include fine-grained crystalline dolostone and two types of coarser grained hydrothermal dolomite, referred to as medium- and coarse-grained crystalline dolomite and later saddle dolomite; the scheme follows on previous work (Qing, 1991, 1998; Qing & Mountjoy, 1994). The base-metal mineralization is sphalerite dominant occluding cavities (Fig. 3b), fine-grained disseminations (Fig. 3a, c), or bands (Fig. 3d). Galena is common and shows variable textural relationships with sphalerite, and is most often paragenetically later (Fig. 3e, f).

General comments on the content of the samples examined follow. Dolomite is the dominant carbonate and present as the four types noted above. Calcite occurs in most settings and is specifically present in the Kootenay Arc samples. Quartz is a late-stage, open-space filling mineral, but also noted to be more abundant in the Kootenay Arc samples, such as the Wigwam deposit. Hematite, barite, and pyrobitumen all post-date sulphides which includes sphalerite, galena, pyrite, marcasite, and chalcopyrite. Sphalerite is the most abundant sulphide except for the Oldman deposit, where galena dominates. Pyrite is noted to be part of the later, post-mineralization–stage cementation. Marcasite is rarely observed - i.e., Wigwam and Abbott-Wagner where it pre-dates pyrite and chalcopyrite - and also as a late fracture-filling event.

Paragenesis

The paragenetic sequences of the sites follows on from extensive previous work (summarized in Kontak *et al*., 2022). Here observations are presented in sequential order, reflecting the geological settings referred to above; we note the many similarities in terms of the timing of dolomitization and the main

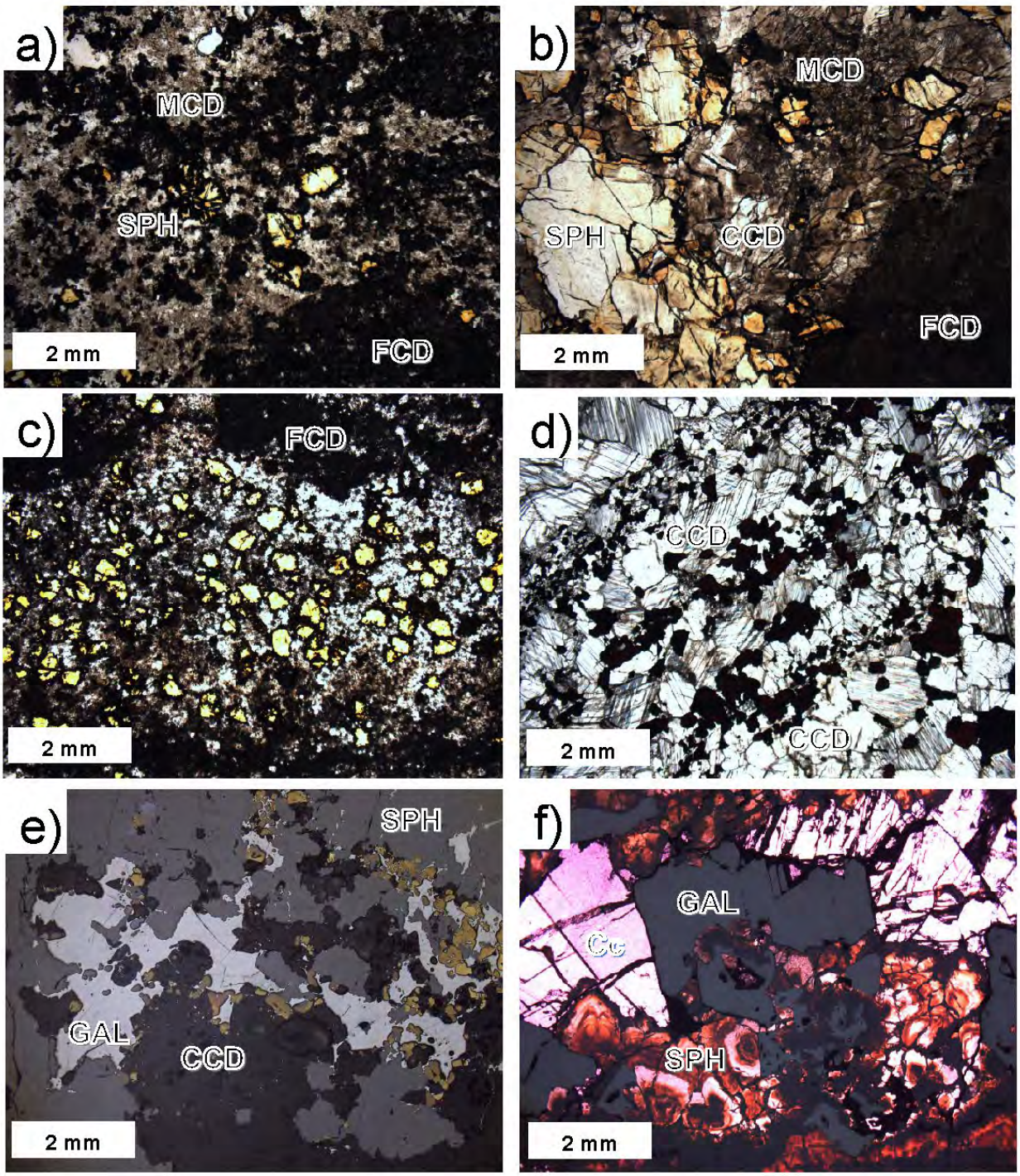

Figure 3: *Typical microscopic textures in host rocks and MVT-type mineralized samples of this study, as seen in transmitted light (TL) and reflected light (RL):* ***a)*** *Shag (TL): mixture of carbonate mineral types with earlier fine-grained crystalline dolostone (FCD) overprinted by colourless, translucent, and dark medium-grained crystalline dolomite (MCD) to coarse-grained crystalline dolomite (CCD) associated with pale yellow-brown anhedral sphalerite (SPH);* ***b)*** *Robb Lake (TL): coarse SPH associated with CCD overgrowing earlier dark MCD, which replaced FCD. The SPH is red-yellow on its margin and translucent and colourless in its core;* ***c)*** *Shag (TL): disseminated, equant, anhedral, pale yellow SPH intergrown with MCD. Note FCD is seen along margins of the mineralization (see Fig.8a, h for close-up);* ***d)*** *Jersey-Emerald (TL): equant SPH intergrown with CCD. This SPH appears pale yellow to orange at higher magnification (see Fig. 7c for close-up);* ***e)*** *Abbott-Wagner (RL): typical coarse-grained, late-stage galena (GAL) cutting earlier SPH and CCD;* ***f)*** *Pine Point (TL, RL): typical coarse-grained, late-stage galena cutting earlier zoned SPH and late-stage, cavity-filling calcite (Cc). Figure is from Kontak et al. (2022).*

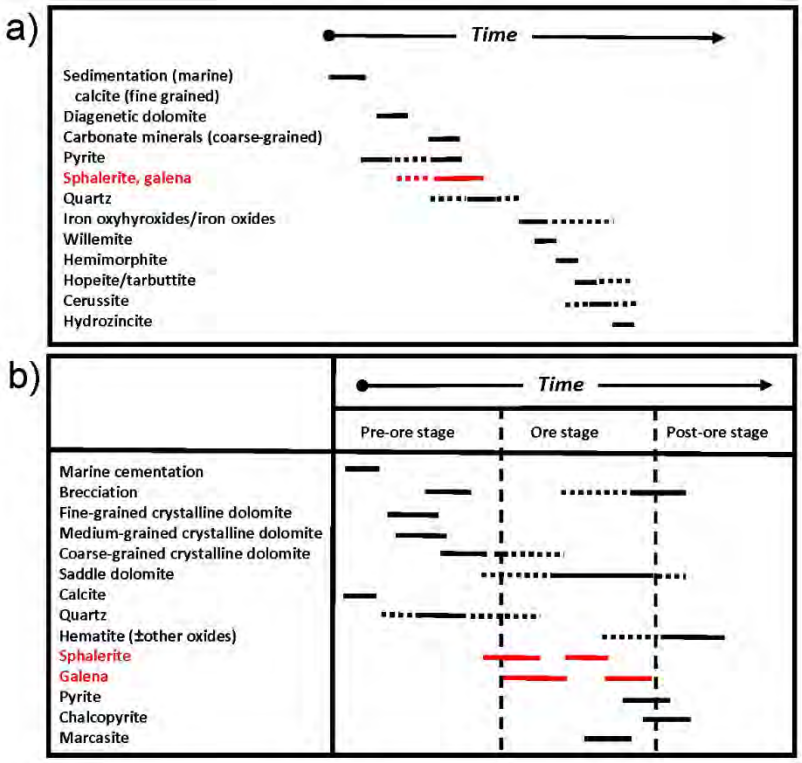

Figure 4: *Mineral paragenesis for Kootenay Arc deposits as proposed by (a) Paradis et al. (2015), and (b) this study based on samples from our study areas and Table 2. Figure is from Kontak et al. (2022).*

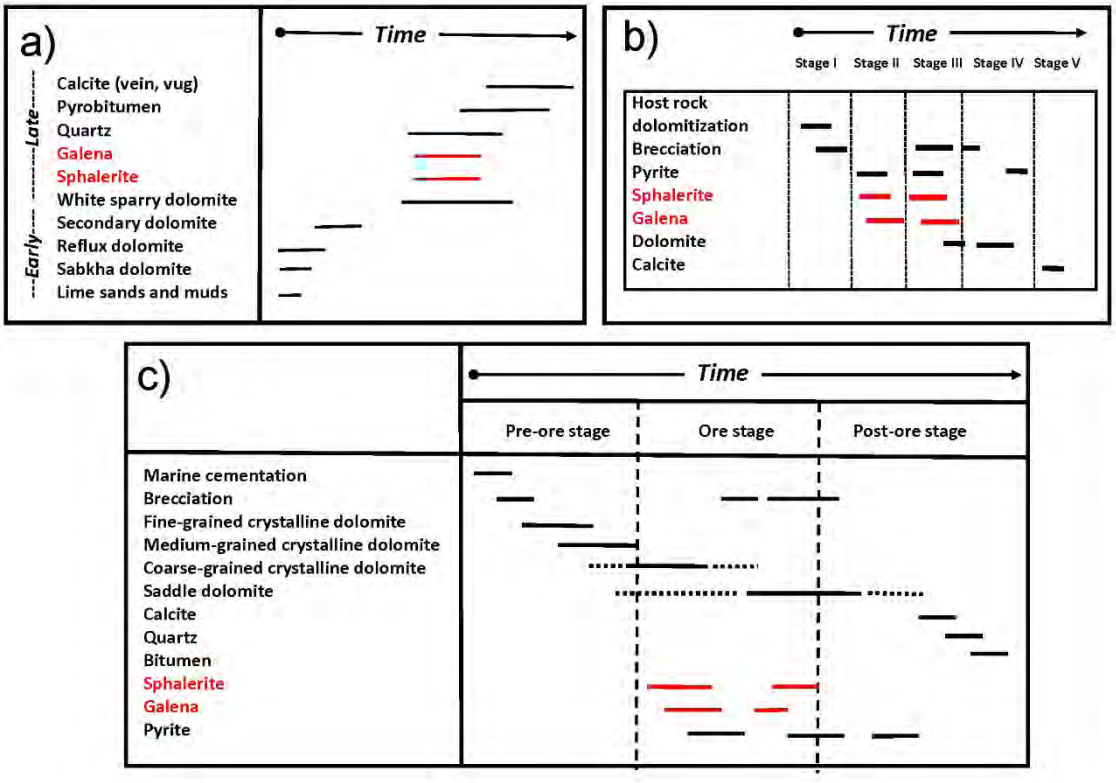

Figure 5: *Mineral paragenesis for studied areas of the Rocky Mountain fold and thrust belt deposits based on* ***(a)*** *Robb Lake (after Macqueen and Thompson, 1978),* ***(b)*** *Kicking Horse and Monarch (after Vandeginste et al., 2007),* ***(c)*** *this study using samples described in the text and in Table 3. Figure is from Kontak et al. (2022).*

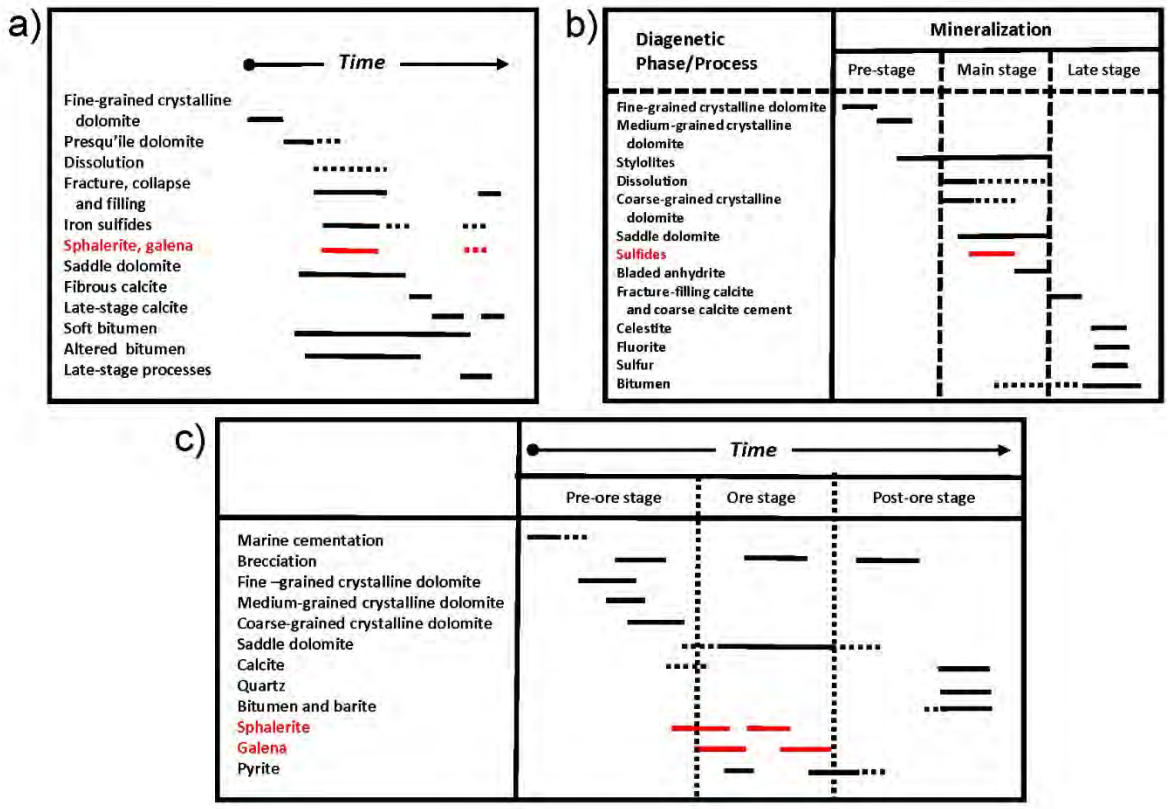

Figure 6: *Mineral paragenesis for various settings in the Western Canadian Sedimentary Basin.* ***(a)*** *Pine Point orebodies after Krebs and Macqueen (1984);* ***(b)*** *Presqu'ile Barrier area after Paradis et al. (2006); and* ***(c)*** *this study based on samples described in the text and in Table 4. Figure is from Kontak et al. (2022).*

mineralizing events. In all cases carbonate occurs as early dolostone, various dolomite phases, and calcite (again note the classification scheme used above) and show a consistent sequence (fine-grained crystalline dolostone to medium-grained crystalline dolomite to coarse-grained crystalline dolomite to saddle dolomite). Sulphides, in order of relative decreasing abundance, are sphalerite, galena, pyrite, marcasite, and chalcopyrite and follow the convention of pre-, syn-, and post-mineralization stages corresponding to the precipitation of sulphide minerals (e.g., Paradis *et al*., 2006). As local deposit variability precludes a single paragenesis, an overall paragenesis is presented for each of the study areas and general features of each area are discussed in sequence and summarized in Figures 4 to 6.

Kootenay Arc

The earlier paragenesis here by Paradis *et al*. (2015; Fig. 4a), described as "carbonate-hosted non-sulphide Zn-Pb occurrences", contrasts to newer observations using samples from several settings (Table 1 and Fig. 4b; Jersey-Emerald, Reeves MacDonald, HB, Abbott-Wagner, Wigwam, Rose, and Mastodon). Most of the differences, specifically lack of identified oxide phases in this study, likely reflects different samples and their locations. In this context, the noted complexity of mineralization among the settings made establishing an overall paragenesis challenging. However, some of the paragenesis is broadly similar to that for the Rocky Mountain samples (see below) with early dolomite, but in contrast much of the ore-stage event being synchronous with the saddle dolomite. Chalcopyrite occurs in several deposits (e.g., Wigwam and Abbott-Wagner), and is paragenetically late.

Rocky Mountains fold and thrust belt

The newer results, which are compared with the previous paragenetic relationships for some of the larger deposits in Figure 5 (i.e., Robb Lake (Krebs & Macqueen, 1984), Kicking Horse, and Monarch (Vandeginste *et al.*, 2007)), also includes observations for three additional settings mentioned above (Shag, Munroe, and Oldman); see Table 2. Our findings closely match the earlier conclusions, but with some differences in timing and classification of carbonate stages noted. Mineralization follows a protracted stage dolomite formation and continues such that is overlaps with the later coarse-grained crystalline dolomite and saddle dolomite types, which are then followed by calcite, quartz, and both bitumen and pyrobitumen.

Western Canadian Sedimentary Basin

Numerous previous studies for this setting reflects the importance of this area, such as the past-producing Pine Point deposits. The newer observations (Fig. 6), which included the many settings noted above (Table 3), are compared to a previous study at Pine Point (Fig. 6a; Krebs & Macqueen, 1984) and the more regional study of the Presqu'ile Barrier (Fig. 6b; Paradis *et al*., 2006). In general, at Pine Point the main sulphide

	Deposit	Reeves MacDonald	Jersey-Emerald	HB	Wigwam	Rose	Abbott-Wagner	Mastodon
	Number of Samples	1	4	1	1	1	1	1
Gangue minerals	FCD	●●●	●●	●●●		●		●
	MCD	●●●	●●		●		●	●●
	CCD	●●	●●●			●		
	SD	●	●●			●	●●	
	Cc	●●	●●●	●●●	●	●●		●
	Qtz	●	●	●	●●●	●		●●
	Hem	●	●●				●●	
	Bar							
	PBit				●			
Ore mineralogy	Sph	●●	●●●	●●●	●●●	●●●	●●●	●●●
	Gal	●					●●	●
	Py	●●	●●	●	●		●●	●
	Cpy				●		●	
	Mrc		●		●	●?		

Present - ● Dominant - ●● Abundant – ●●●

Bar: Barite; Bit: Bitumen; Cc: Calcite, Cpy: Chalcopyrite, CCD: coarse-grained crystalline dolomite; FCD: fine-grained crystalline dolomite; Gal: Galena, Hem: Haematite, Mrc: Marcasite, MCD: medium-grained crystalline dolomite; SD: saddle dolomite, Py: Pyrite, Qtz: Quartz; Sph: Sphalerite

Table 1. *Summary of the mineralogy, gangue, and ore minerals and their relative abundances for samples from the mineralized sites in the Kootenay Arc; note the classification scheme for dolomite types is after Qing (1991). Note that this is modified after Table 2 in Kontak et al. (2022).*

	Deposit	Robb Lake	Monarch	Kicking Horse	Munroe	Shag	Oldman
	Number of Samples	2	3	4	2	7	1
Gangue minerals	FCD	●●●	●●	●●●	●●●		
	MCD	●●	●		●●	●	●●
	CCD	●●	●	●	●●●	●●	●●
	SD	●●	●●●	●●	●●●	●●	●●●
	Cc	●	●	●	●	●	●●
	Qtz				●	●	●
	Hem						
	Bar						
	Bit						
Ore mineralogy	Sph	●●●	●●●	●●●	●●●	●●●	●
	Gal	●	●●	●		●	●●●
	Py	●●	●	●●	●	●	●
	Cpy						
	Mrc						

Present - ● Dominant - ●● Abundant – ●●●

Bar: Barite; Bit: Bitumen; Cc: Calcite, Cpy: Chalcopyrite, CCD: coarse-grained crystalline dolomite; FCD: fine-grained crystalline dolomite; Gal: Galena, Hem: Haematite, Mrc: Marcasite, MCD: medium-grained crystalline dolomite; SD: saddle dolomite, Py: Pyrite, Qtz: Quartz; Sph: Sphalerite

Table 2. *Summary of the mineralogy, gangue, and ore minerals and their relative abundances for samples from the mineralized sites in the Rocky Mountain fold and thrust belt; note the classification scheme for dolomite types is after Qing (1991). Note that this is modified after Table 3 in Kontak et al. (2022).*

	Deposit	Pine Point	Martin Hills	Steen River	Slavey Creek	Dawson oil field	Oak gas field	Great Slave Reef
	Number of Samples	2	1	1	4	1	1	9
Gangue minerals	FCD		●●●	●	●●●	●●●		●
	MCD	●●	●●	●	●●	●●●	●●●	●
	CCD	●			●		●●	●●●
	SD	●●●		●●●	●●	●●	●●●	●●●
	Cc	●		●●	●	●●●	●	●●
	Qtz	●						●
	Hem							
	Bar			●●				
	Bit				●			
Ore mineralogy	Sph	●●●			●●		●	●●●
	Gal	●●		●		●		●●●
	Py	●	●●●	●	●●●	●●●	●	●
	Cpy				●		●	
	Mrc							●

Present - ● Dominant - ●● Abundant – ●●●

Bar: Barite; Bit: Bitumen; Cc: Calcite, Cpy: Chalcopyrite, CCD: coarse-grained crystalline dolomite; FCD: fine-grained crystalline dolomite; Gal: Galena, Hem: Haematite, Mrc: Marcasite, MCD: medium-grained crystalline dolomite; SD: saddle dolomite, Py: Pyrite, Qtz: Quartz; Sph: Sphalerite

Table 3. *Summary of the mineralogy, gangue, and ore minerals and their relative abundances for samples from the mineralized and barren sites in the Western Canadian Sedimentary Basin; note the classification scheme for dolomite types is after Qing (1991). Note that this is modified after Table 4 in Kontak et al. (2022).*

Texture	Definition
Crackle breccia (CB)	Slight displacement of fragments
Mosaic breccia (MB)	Fragments are largely but not wholly displaced
Rubble breccia (RB)	Fragments are completely displaced in both the host rock and sulfides
Pseudobreccia (PSE)	Breccia-like fabric produced by selective replacement of host rock fabric
Rhythmites (RHM)	Rhythmically banded ore containing distinct generations of sphalerite or gangue carbonate mineral(s) that usually develops from cycles of dissolution and open-space filling
Replacement (REP)	Original phase replaced by paragenetically later phase
Colloform (CF)	These are fine-scale (<1 mm), banded sulfides, spherulitic aggregates of colloform sphalerite, and dark bands of fibrous aggregates of crystal
Fine-grained banded ore (FGB)	Fine-scale banding (micron- to millimetre-scale bands) is common in individual crystals and in some deposits
Snow-on-roof (SOR)	Typically consists of sulfides preferentially coating the tops of crystals or breccia clasts in open space

Table 4. *Definitions of the textures observed in host rock and ore phases in samples of Mississippi Valley–type deposits in the southern Canadian Rocky Mountains and the Western Canadian Sedimentary Basin. Note that this is after Table 5 in Kontak et al. (2022).*

	Deposit	Reeves MacDonald	Jersey-Emerald	HB	Wigwam	Rose	Abbott-Wagner	Mastodon
	Number of Samples	1	4	1	1	1	1	1
Host rock textures	CB		●		●		●	
	MB	●				●		●
	RB	●		●				●
Host rock mineralization textures	PSE							
	RHM	●	●					●
	REP	●●	●●	●	●●	●●	●	●
Mineralization textures	CF						●●	
	FGB	●						
	SOR		●		●●			

Present - ● Dominant – ●●

CF: colloform banded, CB: crackle breccia, FGB: fine-grained banded, MB: mosaic breccia, PSE: pseudobreccia, REP: replacement, RHM: rhythmite layering, RB: rubble breccia; SOR: 'snow on roof'.

Table 5*. Summary of the textures observed in the host rocks, mineralized material, and ore minerals based on petrographic study of samples from the Kootenay Arc mineralized districts. Note that this is modified after Table 6 in Kontak et al. (2022).*

	Deposit	Robb Lake	Monarch	Kicking Horse	Munroe	Shag	Oldman
	Number of Samples	2	3	4	2	7	1
Host rock textures	CB	●	●	●●	●●	●	
	MB	●	●	●	●●	●	●
	RB	●	●●	●●	●	●	●
Host rock mineralization textures	PSE	●		●●			●●
	RHM	●	●	●		●	
	REP	●●	●●	●●	●●	●●	●
Mineralization textures	CF	●	●●	●			
	FGB		●	●	●	●	
	SOR		●				

Present - ● Dominant – ●●

CF: colloform banded, CB: crackle breccia, FGB: fine-grained banded, MB: mosaic breccia, PSE: pseudobreccia, REP: replacement, RHM: rhythmite layering, RB: rubble breccia; SOR: 'snow on roof'.

Table 6. *Summary of the textures observed in the host rocks, mineralized material, and ore minerals of samples from the Rocky Mountains fold and thrust belt mineralized districts based on petrographic study. Note that this is modified after Table 7 in Kontak et al. (2022).*

	Deposit	Pine Point	Marten Hills	Steen River	Slavey Creek	Dawson oil field	Oak gas field	Great Slave Reef
	Number of Samples	2	1	1	4	1	1	13
Host rock textures	CB		●		●●	●	●	●
	MB			●	●			●
	RB	●		●	●			
Host rock mineralization textures	PSE				●●			
	RHM	●						
	REP	●●	●	●				●●
Mineralization textures	CF	●●						●●
	FGB	●●						●
	SOR							

Present - ● Dominant – ●●

CF: colloform banded, CB: crackle breccia, FGB: fine-grained banded, MB: mosaic breccia, PSE: pseudobreccia, REP: replacement, RHM: rhythmite layering, RB: rubble breccia; SOR: 'snow on roof'.

Table 7. *Summary of the textures observed in the host rocks, mineralized material, and ore minerals of samples from the Western Canadian Sedimentary Basin barren and mineralized districts based on petrographic study. Note that this is modified after Table 8 in Kontak et al. (2022).*

stage follows a preparatory stage of dolomitization that overlaps with saddle dolomite, which is succeeded by calcite. Importantly, oil and bitumen overlap much of the paragenesis (see below), as also documented by Szmihelsky *et al*. (2020). Paradis *et al.* (2006) noted a similar paragenesis with some notable additions: 1) subdivision of coarse dolomite into coarse crystalline and saddle types; 2) addition of late bladed anhydrite; and 3) recognition of late celestite, fluorite, and native sulphur. Our newer study (Fig. 6c) subdivided the dolomite types and also noted two generations of sphalerite, galena, and pyrite, with sphalerite occurring as 1) disseminations replacing carbonate host rocks; and 2) paragenetically later, massive, coarse-grained aggregates with colloform and botryoidal habits. An acicular or dendritic form of galena, due to rapid growth, is also noted (see below).

Host rock and mineral textures

Previous workers have noted that various textures, both at the macroscopic and microscopic scale, provide insight into physical conditions associated with base- and precious-metal mineralization in various ore settings (e.g., Fowler & L'Heureux, 1996; Leach *et al*., 2005; Moncada *et al*., 2012). Thus, the various textures noted, summarized in Table 4, are presented for the three geological settings in Tables 5 to 7 to ascertain the potential for regional trends. Additionally, representative images of sphalerite mineralization are shown in Figures 7 to 9.

These observations identified nine textures (Table 4) which were separated into host rock, host rock mineralization, and mineralization. The textures observed are divided on a bipartite basis: 1) host rocks and cements; and 2) sulphide mineralization. Host rock textures include various types of breccias (e.g., crackle, mosaic, and rubble), whereas sulphide mineralization textures include colloform, fine-grained banding, and snow-on-roof. Replacement, rhythmite, and pseudobreccia textures are present in both.

Host-rock textures

These features reflect the various breccia types present in all settings. Crackle breccias have minor displacements of gangue fragments, whereas mosaic breccias are largely, but not fully, displaced, and rubble breccias are fully displaced. Both crackle and mosaic breccias consist of mostly angular fragments. These textures are more common in the Rocky Mountain samples and are dominant at the Munroe, Kicking Horse, and Monarch (e.g., Fig. 7a, b) deposits. They are less dominant in the Western Canadian Sedimentary Basin deposits, and even less so in the Kootenay Arc deposits. Rhythmites or layered textures are present at seven sites — four in the Rocky Mountains and three in the Kootenay Arc — but apparently absent in the Western Canadian Sedimentary Basin samples.

Host-rock and sulphide textures

A number of textures related to the host rock, gangue material, and mineralized ore phases are noted. Pseudobreccia was rarely documented – three sites in the Rocky Mountains and one in the Western Canadian Sedimentary Basin. It is related

District	Deposit	Mineral	Stage	FI type	Tm_{Ice} (°C)	N	Th (°C)	N	Source
NE Rocky Mountains	Robb Lake	Sphalerite	Ore Stage	P, PS	-26 to -12	41	87 to 154	105	Sangster and Carrière (1994)
SE Rocky Mountains	Kicking Horse	Sphalerite	Ore Stage	P, NC	-26.4 to -17.1	25	68 to 93	28	Vandeginste et al (2007)
		Gray dolomite	Post ore	P, NC	-27.3 to -17.7	64	101 to 151	106	
		White dolomite	Post Ore	P, PS, NC	-29.7 to -17.2	40	115 to 167	62	
		Coarse dolomite	Post ore	P, PS, NC	-30.5 to -17.4	33	106 to 152	35	
		Reddish dolomite	Post ore	P, PS, S, NC	-28.6 to -7.7	29	103 to 174	38	
		Calcite	Post ore	NC	-19 to -13.9	11	50 to 72	9	
SE Rocky Mountains	Monarch	Sphalerite	Ore Stage	P, PS, NC	-24.8 to -18.6	22	66 to 109	32	
		Gray dolomite	Post ore	P, PS, S, NC	-27.1 to -17.3	64	93 to 146	97	
		White dolomite	Post ore	P, PS, NC	-29.9 to -18.5	58	94 to 142	78	
		Reddish dolomite	Post ore	P, PS, NC	-29.1 to -17.7	36	128 to 193	21	
WCSB	NE BC	Calcite	Post Ore	P,S	-16 to -10	27	135 to 180	35	Qing (1991)
		Quartz	Post Ore	NC	-13.6 to -6.8	10	165 to 211	19	
WCSB	Pine Point	Sphalerite	Ore Stage	P, PS, S	-35 to -4	133	51 to 99	112	Roedder (1968)
		Dolomite	?	P, PS	-19 to -14	4	88 to 100	23	
		Calcite	Post Ore	P, PS	-12 to -0.5	14			
	Pine Point	Sphalerite	Post ore	NC	-30 to -5	34	51 to 99	57	Kyle (1981)
	Pine Point District	FMD	Pre ore	P	-29.1 to -23.7	3	97 to 104	3	Turner (2006)
		Sphalerite	Ore stage	P	-33 to -22.2	9	60 to 108	9	
		CCD	Ore stage	P	-32.5 to -13.6	6	95.5 to 126	6	
		SD	Post Ore	P	-18.5 to -30.6	13	86 to 112.5	13	
		Calcite	Post Ore	P	-11.2 to -0.7	14	62 to 109	14	
	Pine Point	SD	Post Ore	P, S	-23.5 to -14.5	4	75 to 115	24	Qing (1991)
		Calcite	Post Ore	P, S	-5 to -3	8	70 to 130	8	
		SD	Post Ore	P, S	-23.5 to -5.5	32	95 to 175	33	
		SD	Post Ore	P, S	-34 to -5.5	34	105 to 210	74	
	Central Presqu'ile Barrier	Calcite	Post Ore	P, S	-10 to -7	3	85 to 140	6	
	Northern Alberta	FMD	Pre ore	P	-13	1	130.9	1	Turner (2006)
		Sphalerite	Ore stage	NC			116	1	
		SD	Post Ore	P			109 to 124	2	
		Calcite	Post Ore	NC	-9.6	1	101	1	

CCD: coarse-grained crystalline dolomite; FMD: fine- to medium-grained crystalline dolomite; FI: fluid inclusions type (SD: saddle dolomite; FI type: NC: not classified; P: primary; PS: pseudosecondary; S: secondary; N: number measurements; NE/SE RMFTB: northeast or southeast Rocky Mountain fold and thrust belt Th: homogenization temperature; Tm_{ice} = melting temperature of ice; WCSB: Western Canadian Sedimentary Basin

Table 8. *Summary of fluid inclusion data from previous studies of Mississippi Valley–type deposits in the southern Canadian Rocky Mountains and the Western Canadian Sedimentary Basin. Note that this is after Table 1 in Kontak et al. (2022).*

to both earlier dissolution features (e.g., cavities lined by carbonate and sulphide) and post-ore deformation. Replacement textures are common throughout the study areas, except for five sites in the Western Canadian Sedimentary Basin. As noted, rhythmites (Fig. 3d) occur in seven samples for sites in the Rocky Mountains and Kootenay Arc but absent in all the Western Canadian Sedimentary Basin samples.

Sulphide textures

Sphalerite dominates the sulphides in most samples and thus particular attention was given to its occurrence and nature for which considerable variation is noted in regard to grain size, texture, habit, and colour (Figs. 7, 8 and 9a, b). At the macroscale such mineralization is highly variable as disseminated or isolated grains (Figs. 3a, c, 7c, 9a, b) to partly connected (i.e., net-textured; Fig. 3d, 7d, e, f, 9c) through to massive (Fig. 9d, e). Additionally, it can occlude cavities (Fig. 3b, f, 7g, h, i, 9c), form replacement, or single or multiple layers. The latter banding can be a primary feature of ores (e.g., colloform at Pine Point (Fig. 7i, 8) and Great Slave Reef, Monarch (Fig. 7 b) and Kicking Horse (Fig. 7j)) or as a distinct banding (Fig. 3d) related to post-ore recrystallization. Post-ore brittle brecciation is common (Fig. 7a, e.g., Monarch, Kicking Horse, Monroe), with lesser ductile fabrics also noted, referred to above as pseudobreccia and evidenced as augen-like features at Shag. Rarely there occurs a halo of fine-grained sphalerite in the host carbonate matrix; less so coarser grains display tentacle-like apophyses extending into the matrix where fine-grained sphalerite occurs (Fig. 9c). The latter feature relates in part to the texture of the carbonate minerals; coarse-grained crystalline dolomite commonly surrounds this type of sphalerite and may be a dissolution and precipitation feature (e.g., Fig. 9a, b, f; Putnis, 2009).

At the microscale, sphalerite varies considerably and reflects both primary features, such as faint to strong colour zoning (Fig. 7g, i, 9g, h) and colloform banding (Fig. 7b, I, 8a-d), or overprinting processes (e.g., recrystallization; Fig. 7k, l). Intergrowth of sphalerite with coarse carbonate that defines banded ore (Fig. 4d) is a late feature. Well-developed anisotropy (Fig. 7m, n, 9i) is common, even though other textures indicative of deformation are lacking; it is absent in sphalerite for Mastodon samples. A fine wispy lamination of opaque material, whose origin is unknown, in optically clear sphalerite (Fig. 9j) is only seen in Abbott-Wagner samples.

Brecciation, a common feature at different spatial scales, was noted which indicates post-mineralization comminution. It includes fragmentation of sphalerite with cementation (Fig. 7a, b) or extensive fracturing in place, as in a crackle breccia (Fig. 7k, l).

Rarely observed was snow-on-roof, which is useful as a paleotops indicator (e.g., Leach *et al.*, 2005); it was noted in three samples from Wigwam in the Kootenay Arc. The infilling of radial cracks in fine-grained, banded sphalerite by galena and calcite is rare and only noted at Pine Point (Fig. 8a), as was also observed by Roedder (1968a). Of particular note in regard to the latter is the dendritic and hopper like habits of the galena (Fig. 8h, i), features generally attributed to rapid precipitation and growth.

Sphalerite colour varies considerably and ranges from clear through pale yellow and brown to dark shades of red and brown; this sequence occurs regardless of geographical sampling. The corresponding composition of these different-coloured varieties was not monitored in this study and is not further discussed.

Cathodoluminescence (CL)

Results from preliminary CL microscopy for select samples from Kicking Horse, Jersey-Emerald, Robb Lake, and Slavery Creek settings was used to study the paragenesis of carbonate phases and how it relates temporally to mineralization. As CL relates to excitation of electrons due to specific activators (e.g., Fe, Mn, rare-earth elements [REE]), it can potentially track chemical changes in an evolving chemical system. Long used to study carbonate diagenesis (e.g., Meyers, 1974; McLemore & Barker, 1987), CL is now widely applied to hydrothermal systems (e.g., Götze, 2012; Götze *et al.*, 2013).

The CL results of four imaged samples presented below are attributed to varied Fe contents of the host carbonate based on SEM-EDS analysis, but we note that low levels of REEs could not be identified due to detection limits. Importantly, the images reveal hydrothermal alteration along with multiple stages of carbonate and sulphides, which are readily recognized using routine petrography and thus indicate the application of such imaging to better understand mineral paragenesis in these and other similar settings.

In general, images show early, fine-grained crystalline dolostone and medium-grained crystalline dolomite are CL dull (Fig. 10a) with later coarse-grained crystalline dolomite and saddle dolomite types being CL bright (Fig. 10a, b, c). Additionally, these CL-bright phases are noted to likely occlude space generated via earlier dissolution of matrix carbonate. Also, the CL red and blue seen in the latter images are attributed to variable Fe contents. The CL images also clearly reveal that the coarse carbonate phases record the later development of hydrothermal carbonate minerals at the expense of the earlier matrix carbonate material. That the later carbonate infills porosity generated in the former carbonate suggests that the passage of hydrothermal fluids through the samples generated space via dissolution of the host rock. The latest mineral phase noted is a CL-dull calcite that occludes porosity (Fig. 10d).

A further important feature of the CL images is the presence of sphalerite, which has a bright lime-green luminescence. It occurs as either disseminations in the fine- and medium-grained crystalline dolomite phases (Fig. 10a) or coarser crystals occluding porosity and overlapping growth of coarse-grained crystalline dolomite (Fig. 10c) and saddle dolomite phases. Lastly, the sphalerite appears to outline a halo of sphalerite in the matrix to the coarser dolomite phases.

Carbonate mineral chemistry

A total of 109 SEM-EDS analyses were completed for major- (Ca, Fe, Mg) and minor- (Mn element abundances in textural varieties of dolomite and calcite. Full details are presented in Kontak *et al*. (2022) and the results are summarized below. All

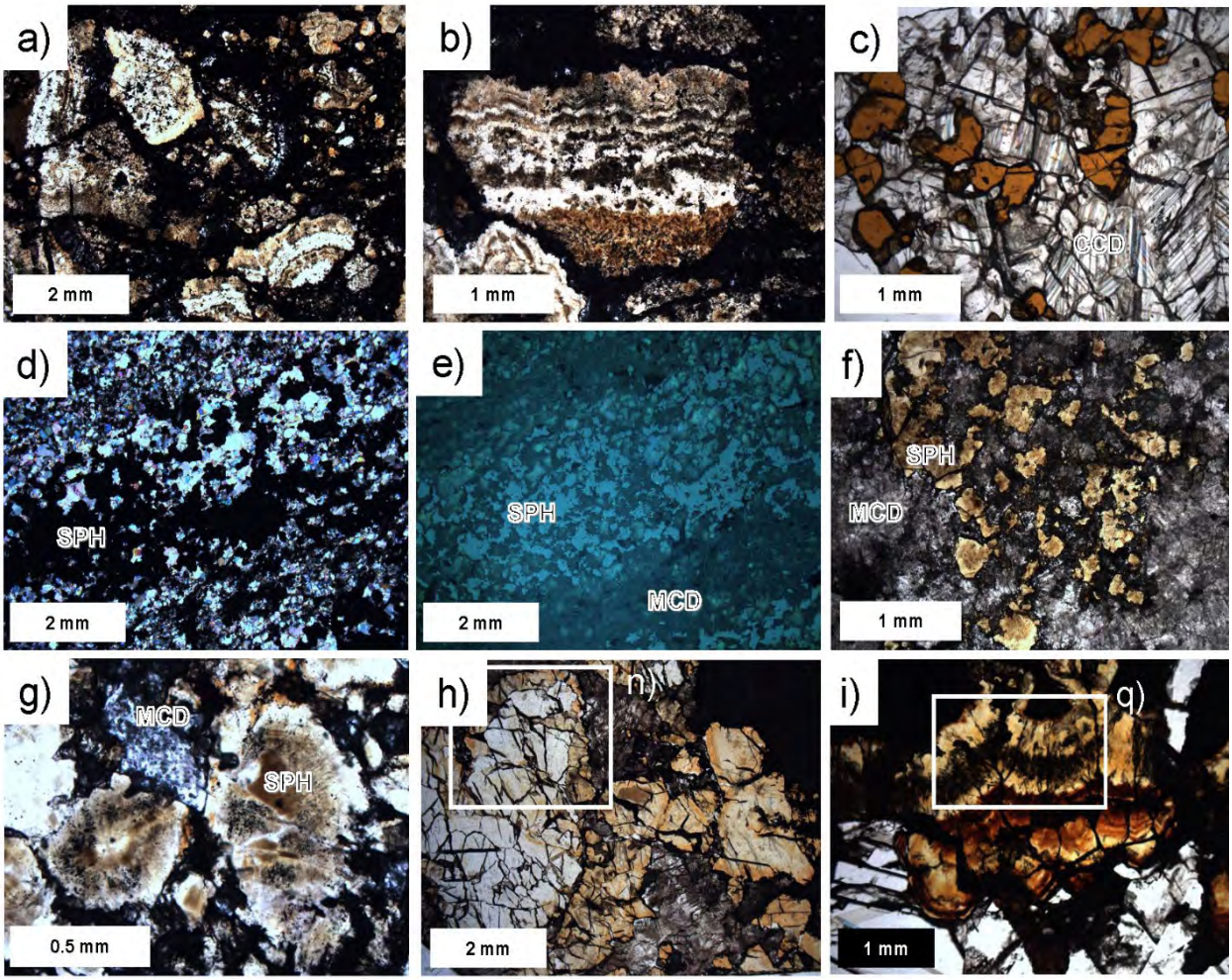

Figure 7: (above and opposite) *Photomicrographs of sphalerite (SPH) mineralization in the studied deposit settings seen in transmitted light (TL), reflected light (RL), and crossed nicols (CN):* ***a) Monarch*** *(TL): brecciated clasts of SPH in a carbonate matrix, with notable variation in the banding, colour, texture, and grain size of SPH;* ***b) Monarch*** *(TL): breccia clast of banded SPH–carbonate mineralization;* ***c) Jersey-Emerald*** *(TL): close-up of banded ore showing intergrowth of yellow-brown, anhedral SPH with coarse-grained crystalline dolomite (CCD);* ***d) Reeves MacDonald*** *(CN): intergrowth of subhedral to anhedral SPH and medium-grained crystalline dolomite (MCD);* ***e) Reeves MacDonald*** *(RL): anhedral sphalerite intergrown with MCD as a vein-like feature;* ***f) Kicking Horse*** *(TL): disseminated, subhedral, zoned, pale yellow-brown SPH intergrown with MCD. Finer-grained SPH around the coarse grains is represented by the dark material;* ***g) Kicking Horse*** *(TL): close-up of image (f) showing zoned, clear to brown SPH and MCD. Note dark areas in SPH are full of fluid inclusions;* ***h) Robb Lake*** *(TL): coarse-grained, subhedral, zoned pale to yellow SPH intergrown with CCD; white box is enlarged in image (n);* ***i) Pine Point*** *(TL): colloform-textured, pale yellow to red-brown SPH; white box enlarged in image (q);* ***j) Kicking Horse*** *(TL): banded/colloform-textured, colourless, translucent, red-brown to pale brown SPH. White box is enlarged in image (q);* ***k) Munroe*** *(TL): anhedral, pale yellow to clear SPH with breccia texture that is cemented by fine-grained carbonate minerals;* ***l) Munroe*** *(TL): close-up of image (k) showing anhedral pale yellow to clear SPH;* ***m) Kicking Horse*** *(CN): coarse-grained SPH with anisotropic behaviour due to strain;* ***n) Robb Lake*** *(CN): close-up of area in image (h) showing subdomains and deformation twin lamellae in SPH surrounded by CCD****; o) Kicking Horse*** *(TL): close-up of image (j) showing abundant, irregular-shaped, fluid inclusion forming in part along the interface of different coloured SPH and at terminations of crystals (see black arrows);* ***p) Kicking Horse*** *(PL): close-up of image (o) showing irregular-shaped, opaque fluid inclusions, the largest of which resembles decrepitate-types;* ***q) Pine Point*** *(TL): close-up of image i) showing band of pale yellow SPH characterized by abundant, elongate fluid inclusions, in part petroleum (see text). Inset shows a close-up of these features. Figure is from Kontak et al. (2022).*

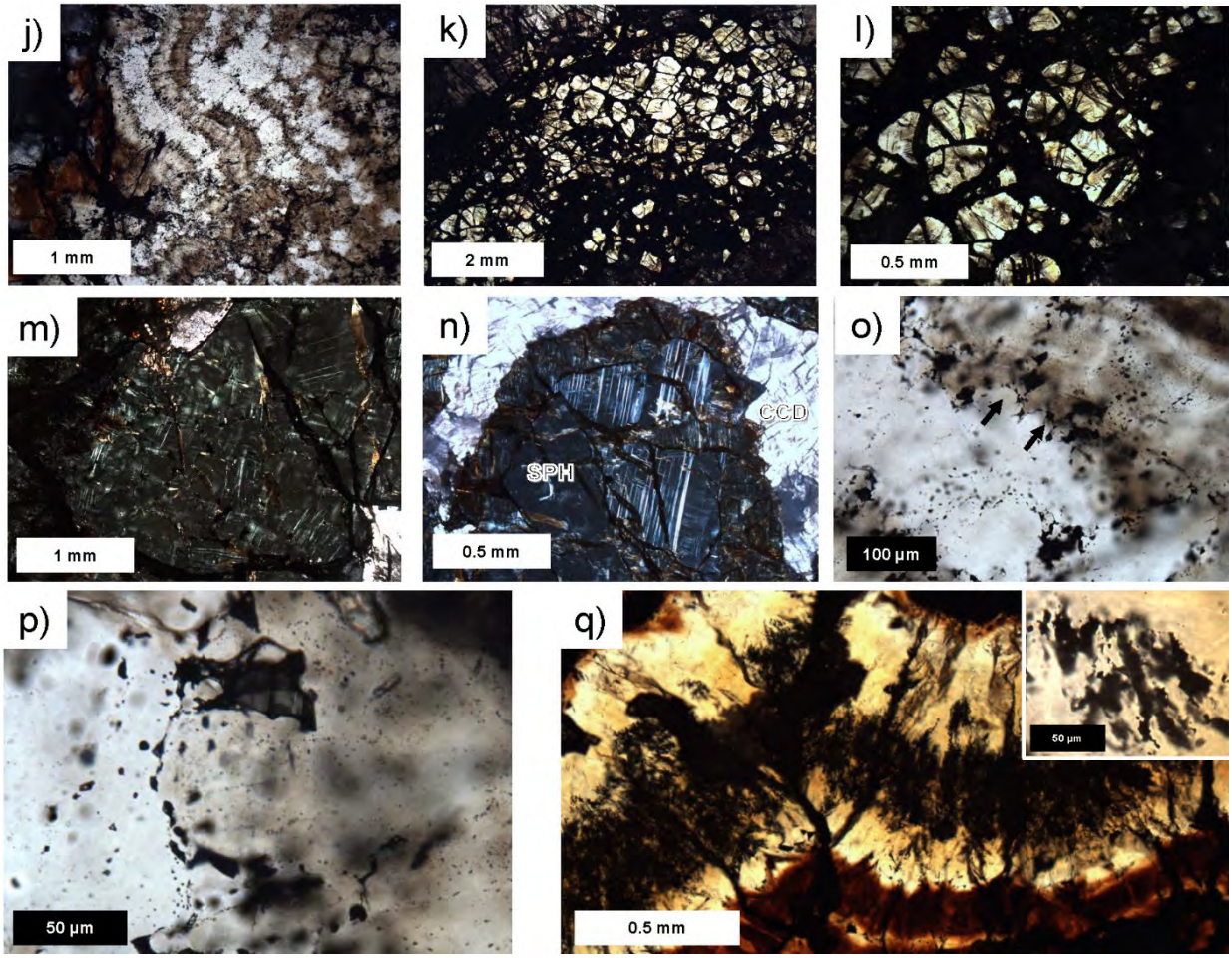

Figure 7 (contd)

the dolomite types identified petrographically have similar chemistries - MgO ranges from 25.3 to 32.8 wt. % CaO from 17.6 to 30.2 wt. %; the Mg-Ca ratios vary from 0.51 to 0.86. The late-stage calcite is Fe free but has up to 10 mol % $MgCO_3$. Data also revealed further distinct geochemical differences among the dolomite types:

- fine- and medium-grained crystalline dolomite, which are texturally similar, have similar chemistries and both are generally Fe poor.
- coarse--grained crystalline dolomite falls into two groups, one Fe free and the other with up to 5 mol % $FeCO_3$.
- saddle dolomite is the most Fe enriched (to 3.3 wt . % FeO; 5–10 mol % $FeCO_3$), with some overlap with the Fe-bearing coarse-grained crystalline dolomite; and:
- MnO was only present in the coarse-grained crystalline dolomite and saddle dolomite types.

Fluid inclusion study

Fluid inclusions (FI) provide the only direct record of the presence of palaeo-hydrothermal fluids and are therefore a valued and widely applied research tool in ore deposit studies. As FI protocols have changed over the years, Kontak *et al*. (2022) discussed the relevance of this to the current study noting in particular: 1) classification; 2) necessity of using the fluid inclusion assemblage (FIA) approach (Goldstein & Reynolds, 1994; Bodnar, 2003a); and 3) assessing data for possible post-entrapment changes, which are addressed below. Here is summarized the results of previous work in the different settings along with results from Kontak *et al.* (2022).

Previous fluid inclusion work

Fluid inclusion studies of mineralization (i.e., sphalerite) and gangue (dolomite, calcite) in relevant areas are summarized in Table 8 for ice-melting temperatures (i.e., Tm_{ice}), salinities, and homogenization temperatures (T_h; in °C). Results of all earlier studies indicate wide variation in Tm_{ice} across the study areas (–35 to –0.5°C), and thus a range in salinities (0.8–28.5 wt. % equiv. NaCl), in addition to the presence of divalent cations (e.g., Ca, Mg). All studies cited metastability issues and lack of freezing, which is not uncommon for saline brines (e.g., Wilkinson, 2017). Given the large range in T_h values (50 to 211°C) in different minerals and noting the lack of the FIA approach, such high T_h values compared to those typical of MVT mineralization (i.e., 75 to 175°C; Basuki & Spooner, 2004; Bodnar *et al.*, 2014) may reflect post-entrapment modification. To address the latter issue, Kontak *et al.* (2022) used results from the

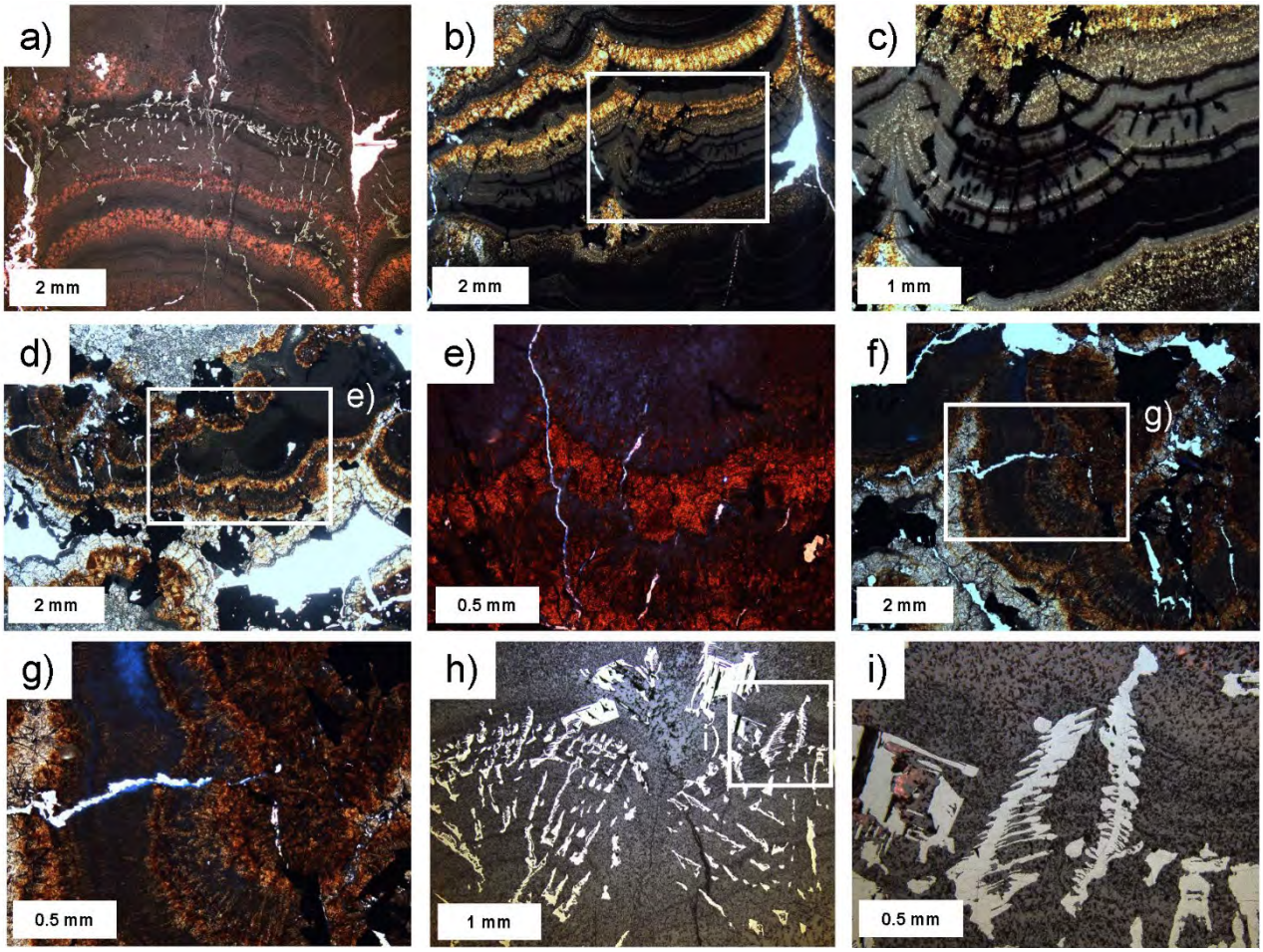

Figure 8: *Photomicrographs of sphalerite (SPH) mineralization in the Pine Point deposit setting seen in transmitted light (TL), reflected light (RL), and ultraviolet light (UV). These images show several features of the SPH: a) banded and colloform-textures (images a, b, c, d); 2) varied colours in TL from red-brown to pale yellow; c) both fine crystalline versus very fine-grained SPH, as seen in images a to d; d) presence of petroleum/bitumen as seen using UV light; note this material is seen in the dark layers of banded SPH (images d to g); and e) late-stage cross cutting veinlets of calcite and acicular to dendritic galena as seen in RL images h and I, and also TL image e.*

extensive study of Vandeginste *et al.* (2007) for the Kicking Horse and Monarch MVT settings to assess the quality of the data and noted large overall ranges for both T_h and Tm_{ice} per host/stage with variation of <5°C to >60°C per group. In particular was the increase in T_h as the range (i.e., variance) of a population increased; it was concluded the likely T_h for sphalerite stage was <100°C with the anomalous high T_h value due to post-entrapment changes. It is also noted that the same interpretation applies to the anomalous high T_h values reported by Qing (1991) and Qing & Mountjoy (1992) for Pine Point and regionally for the Western Canadian Sedimentary Basin.

In contrast to T_h data, the Tm_{ice} data, which is a proxy for salinity, is not modified due to post-entrapment changes. Thus, the variation for Tm_{ice} noted In Table 1 is real and indicates a large range in fluid salinity. However, as much of these data were not collected using the modern FIA protocol it is not possible to be certain if the salinity ranges overlap in time (i.e., syn-mineralization) or represent a later trapping of fluids with varying salinities which is relevant in regard to deposit formation (e.g., fluid mixing).

Types and characteristics of fluid inclusions

The focus of this study were fluid inclusions ('Fls') hosted in ore-stage sphalerite. In general sphalerite hosted abundant FIs (Fig. 11a, b, c, d, e, f); however, for most samples their size (≤5 um) and opacity (e.g., Fig. 11b, d (inset), g, h) made collecting microthermometric data challenging.

Where phases were unambiguously determined, most FIs are two-phase aqueous type (V+L; Fig. 11f, i). Halite, a not uncommon phase for FIs in MVT settings, was not identified, but solid phases (likely mica based on optical properties) were noted and attributed to accidental trapping (Fig. 11i). Examination if FIs under UV light did not reveal liquid petroleum, which can be common in in MVT deposits (Leach *et al.*, 2005), except at Pine Point where it can be abundant and extensive in finer-grained layers of banded sphalerite (Fig. 8d-g) and which is more extensively discussed by Szmihelsky *et al.* (2020). Lastly, cooling (to –180°C) of what appeared to be monophase dark inclusions was done to check for the presence of COH phases, but no evidence of this was noted.

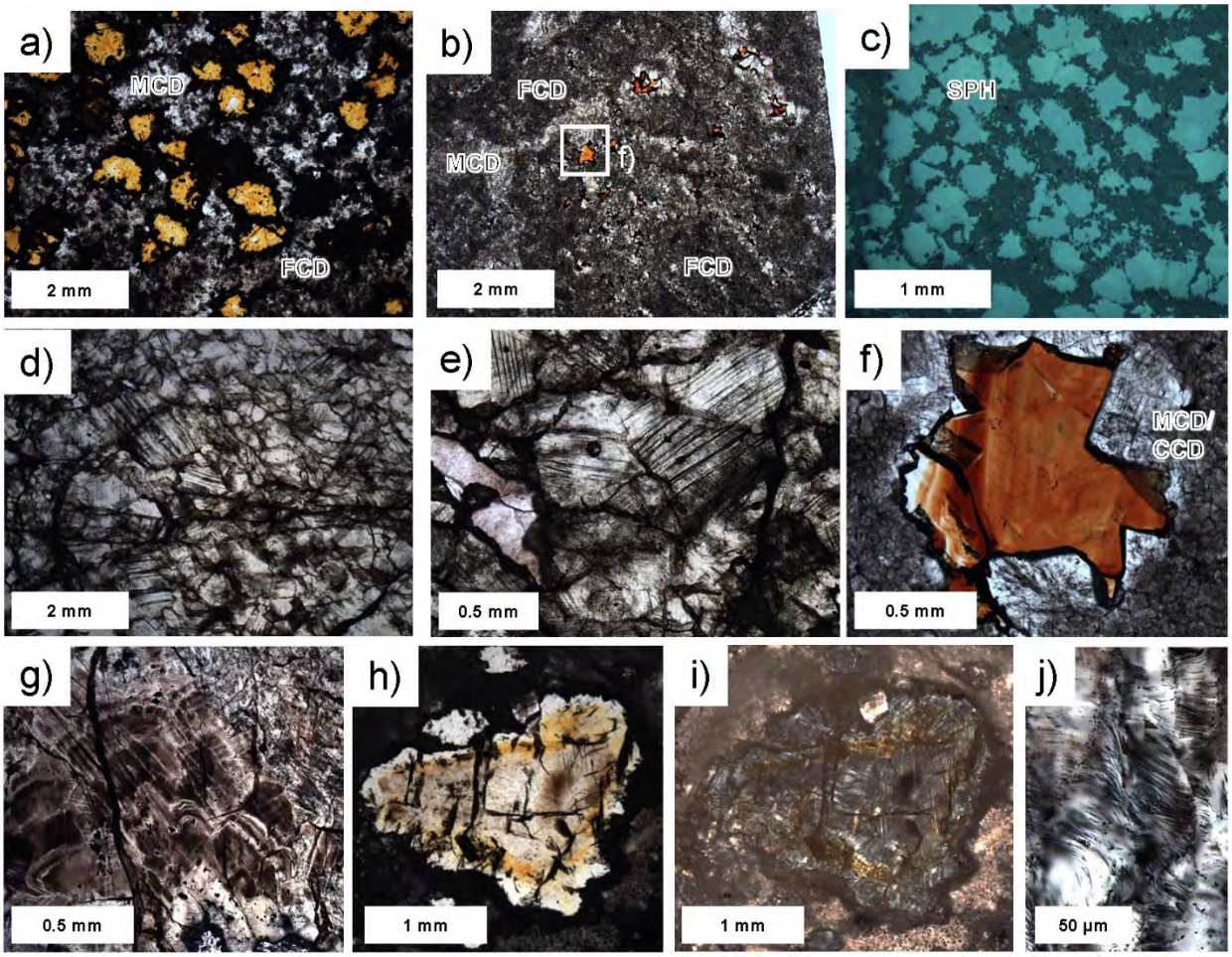

Figure 9: *Photomicrographs of sphalerite (SPH) mineralization in the studied deposit settings seen in transmitted light (TL), reflected light (RL), and crossed nicols (CN):* ***a) Shag*** *(TL): disseminated equant, anhedral grains of pale yellow SPH intergrown with colourless, translucent fine-grained crystalline dolostone (FCD) and coarser grained, dark, medium-grained crystalline dolomite (MCD);* ***b) BM*** *(TL): pale red-brown, anhedral SPH disseminated in colourless, translucent MCD that cuts FCD; white box is area enlarged in image (f);* ***c) Shag*** *(RL): same sample seen in image a) showing the sphalerite (SPH) has a texture of tentacle-like apophyses that partially extend into the matrix****; d) Rose*** *(TL): recrystallized, coarse-grained, colourless, translucent SPH with subgrain development and extensive cross-cutting fractures;* ***e) Rose*** *(TL): close-up of image (d) showing deformation lamellae in SPH that include submicron-sized opaque fluid inclusion;* ***f) BM*** *(TL): close-up of image (b) showing that area around SPH is filled with MCD and coarser grained crystalline dolomite (CCD) that are considered to be pre- to syn-sphalerite;* ***g) Abbott-Wagner*** *(TL): pale brown to colourless, zoned SPH with colloform habit overgrown by finer-grained SPH; See image(j) for higher magnification;* ***h) Shag*** *(TL): anhedral, pale brown and yellow to colourless SPH;* ***i) Shag*** *(CN): same area as in image (h) showing SPH sphalerite is strongly anisotropic with deformation lamellae;* ***j) Abbott-Wagner*** *(TL): pale brown to colourless SPH characterized, at high magnification, by wispy alignment of an unidentified fine-grained opaque material. Figure is from Kontak et al. (2022).*

The FIs observed equate to primary, pseudosecondary, secondary, and indeterminate types (see Bodnar, 2003a). Primary types defined growth zones (Fig. 11a, c, e) or occur as dense clusters coring sphalerite (Fig. 11b, c, f); these are rarely equant (Fig. 11d, f, j) and more commonly irregular shaped (Fig. 12b). Most FIs are secondary (Fig. 11j, k) but where decorating planes of limited extent are considered pseudosecondary (Fig. 11g). The largest FIs were noted to occur at intersecting planes (Fig. 11i, j). Indeterminate types (i.e., one or more isolated inclusions) not related to growth zones or planes and defining 3-D arrays (Fig. 11h, l, m, n, o) vary from irregular to equant.

Atypical shaped FIs were documented at Kicking Horse and Pine Point deposits. At Kicking Horse such FIs define primary growth zones (Fig. 7j) and decorate sphalerite crystals (Fig. 7o, p). They vary in size (<5 µm to 50–70 µm), with larger ones being V-rich based on the presence of a V-L meniscus. Their very irregular shapes, in addition to atypical V-rich nature, suggests they may be decrepitates, which commonly reflect pressure changes (Bodnar, 2003b). At Pine Point, such atypical FIs inundate dark growth zones in colloform-banded sphalerite (Fig. 7i, q) and are characterized as: 1) defining primary growth bands; 2) having a dendritic-like texture; and 3) being elongate and parallel to inferred growth of the host sphalerite.

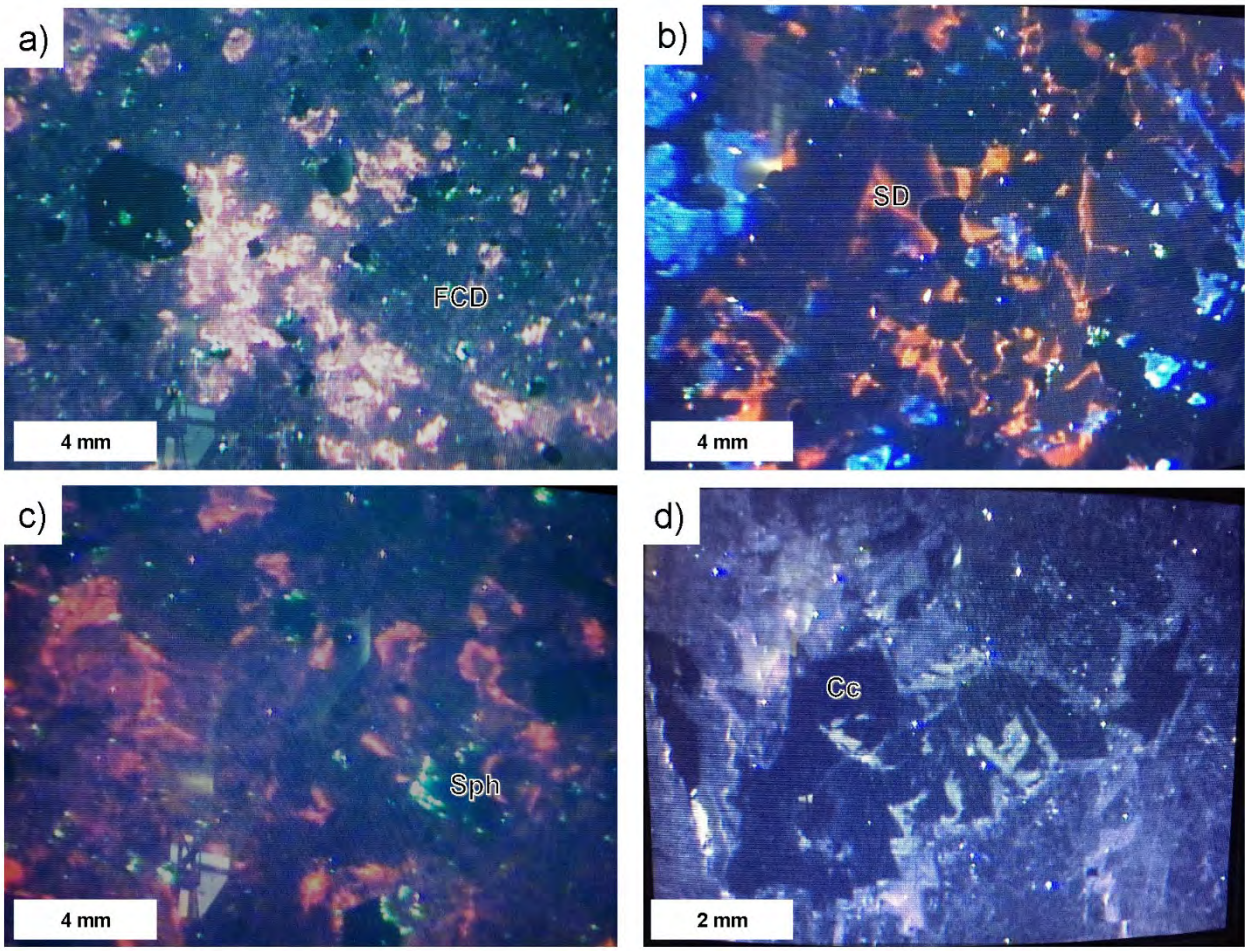

Figure 10: *Cathodoluminescence (CL) images of carbonate samples from mineralized showings.* ***a) Kicking Horse****, southern Canadian Rocky Mountains: note abundant sphalerite, as disseminated CL-bright green phase, within CL-dark fine-grained host dolomite (FGD). The CL-bright pinkish phase is hydrothermal carbonate, which accompanied the dissolution of the host rock, and the dark euhedra is pyrite.* ***b) Jersey-Emerald*** *deposit, Kootenay Arc: variable CL brightness and colours (reddish and bluish) indicate the coarse carbonate phases, possibly saddle dolomite (SD), have differing chemistries;* ***c) Robb Lake*** *deposit, northern Canadian Rocky Mountains: CL-bright red carbonate of hydrothermal origin is proximal the CL-bright green phase, which is sphalerite (Sph).* ***d) Slavey Creek*** *deposit, Western Canadian Sedimentary Basin: variably CL-bright carbonate that is zoned with the brightest phase outlining a cavity now occluded by late-stage CL-dark calcite (Cc). Figure is from Kontak et al. (2022).*

These features are somewhat similar to FIs noted in rapid growth zones of quartz from epithermal settings (e.g., Bodnar *et al.*, 1985). Also, it in some cases these dark FIs did fluoresce under UV light. Thus, they are in all respects like the bitumen-bearing FIs shown in Szmihelsky *et al.* (2020).

The size and shape of the fluid inclusions are noted to vary considerably. The sizes range from sub-micron to tens of microns, and very rarely 100 to 200 µm, within the same sample and also a FIA (Fig. 11h, j, m, o). Shapes are also highly variable from equant to more irregular (Fig. 11b, d, j). Necking is widespread which resulted in a wide variety of inclusion shapes in single FIAs.

Most FIs in sphalerite appear opaque, unless where flat and thin, which hindered collection of microthermometric data; this is noted to occur even for the same FIA (e.g., Fig. 11i, j). Importantly, that the sphalerite in these settings formed at low temperatures (see microthermometric data below) is consistent with their high fluid densities (i.e., >0.95 g/cm^3) and presence of small V phases which the opacity of FIs obscured. The same problem also applies to accurately determining first melting and final ice melting temperatures (Tm_{ice}).

Microthermometric measurements

The microthermometric data collected is summarized in Figure 12; as noted above, the limited data reflects the opacity of FIs. Full details are discussed in Kontak *et al*. (2022).

Cooling runs indicate salinities between 1 and 28 wt. % equiv. NaCl, but for single deposits and occurrences a more restricted range is noted, except for Mastodon where 4 to 23 wt. % equiv. NaCl is noted. These narrow ranges may, however, relate to the limited amount of data collected. Salinity values also do not correlate with inclusion type . Additionally, as hydrohalite and ice melting relationships could not be observed, estimates of bulk chemistry (i.e., Ca:Na ratio) are lacking; however, that

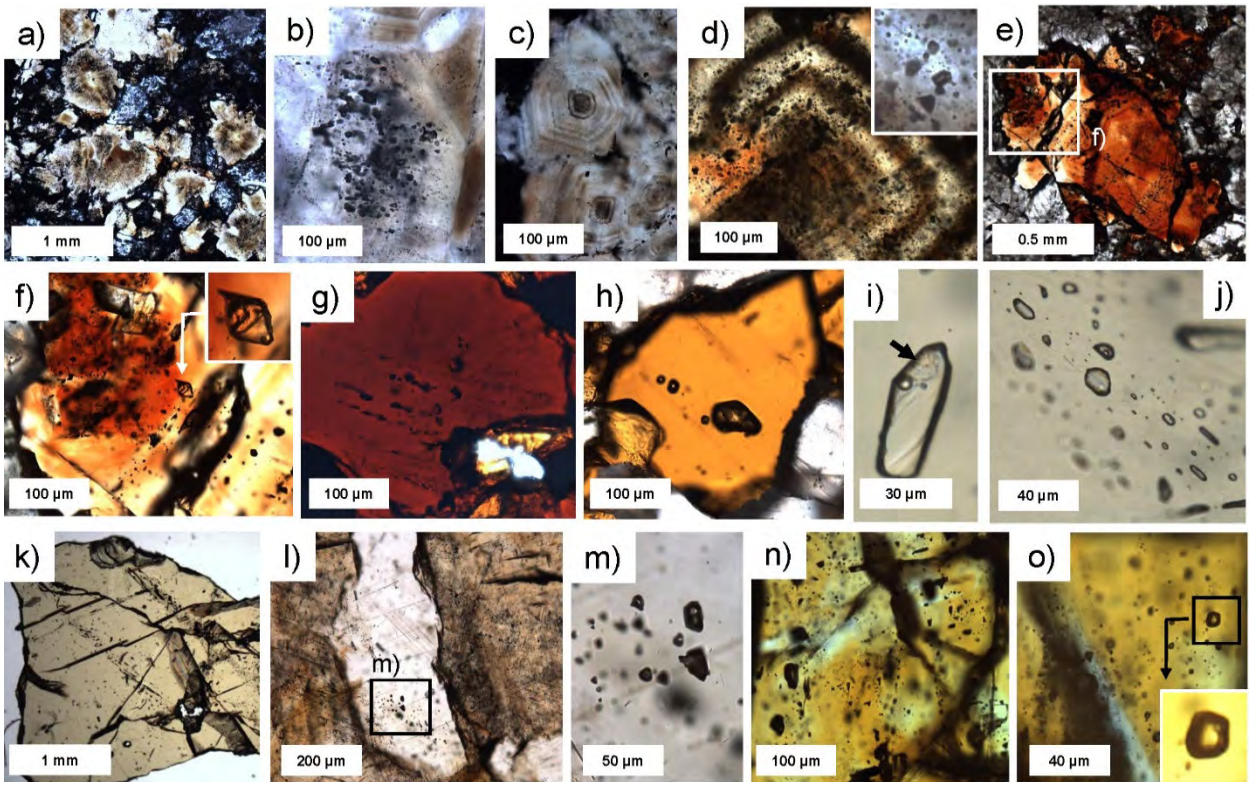

Figure 11: *Photomicrographs in transmitted light of fluid inclusions (FI) hosted in sphalerite (SPH) from studied deposits and districts. The FI are classified as primary (P), pseudosecondary (PS), secondary (S), or indeterminate (I). a) Ki**cking Horse**: subhedral brown-yellow to colourless SPH with P-type FI defining growth zones; b) **Kicking Horse**: close-up of image (a) showing a primary growth zone full of irregular-shaped opaque FI; c) **Monarch**: euhedral, zoned pale brown to colourless SPH crowded with opaque P-type FI; d) **Monarch**: colourless to red-brown zoned SPH inundated with irregular-shaped FI of P, S, and I origins. The inset image is a close-up of opaque FI; e) **BM**: subhedral zoned red-brown to colourless SPH with P- and S-type FI. Area outlined by the white box is enlarged in image (f). f) **BM**: zoned red-brown to clear sphalerite with P- and S-type FI. Note the enlarged FI (denoted by white arrow) with a low vapour (V) to liquid (L) ratio and thus a low Th value (<80°); g) **Jersey-Emerald**: subhedral red-brown SPH with opaque PS-type FI in the core area; h) **Jersey-Emerald**: pale yellow SPH with large, irregular-shaped opaque I-type FI; i) **Mastodon**: colourless SPH hosting an unusually large FI with low V-L ratio, hence low-temperature origin, and an accidentally trapped solid inclusion of mica (indicated by arrow); j) **Mastodon**: colourless SPH hosting plane of S-type equant- to negative-shaped FI that either have low V-L ratios or are opaque; k) **Mastodon**: this colourless SPH chip, which was used for microthermometry, shows planes of S-type FI with low V-L ratios (see images i) and j)); l) **Robb Lake:** colourless SPH bounded by pale yellow-brown SPH, with the former having opaque, PS-type FI. The colourless SPH may be a later generation than the brownish type; area of black box is enlarged image (m); m) **Robb Lake**: opaque PS-type equant FI in clear SPH; n) **Shag**: colourless to yellow, zoned sphalerite hosting small to large, equant I-type FI defining 3-D arrays. Most of the FI are opaque; o) **Shag**: yellow SPH with I-type FI defining 3-D array. Although most FI are opaque, one with a small V phase, outlined by black box, is enlarged in the inset image. Figure is from Kontak et al. (2022).*

some Tm_{ice} values are < -21°C, combined with low freezing and first melting, indicates divalent cations in solution (Wilkinson, 2017). As clathrates were absent, it is likely that dissolved volatiles (C-O-H) are absent (Roedder, 1984).

The Th values show a wide range (77–214ºC), as previous researchers also noted (Table 8). The largest amount of data for a setting is for Mastodon where two populations for T_h are noted: 145 to 147°C and 188 to 214°C. These high T_h values contrast with other settings but for a single value of 187°C for the Shag deposit.

In addition to the conventional T_h values noted above, we used estimated V-L ratio of FIs to infer T_h based on the temperature-density plot for the H_2O system (Roedder, 1984; also see Klyukin *et al.*, 2019). This approach was widely applied for FIs in polished thin sections because their thinner nature (i.e., 30 µm) which circumvented the opacity issue noted above. Using this approach for flattish FIs it was possible to obtain substantially more T_h data (Fig. 13) and indicated a range from <80 to 200°C. Several points are worth noting: 1) for any one FIA, the estimated T_h values are much lower overall ranges for the same sample; 2) where both estimated and measured T_h values are available (e.g., Robb Lake), they agree; and 3) overall the two datasets agree and thus supports the distribution of data in Figure 12. Most important is that the highest estimated T_h values (Fig. 13) for Mastodon and Shag agree with actual measured T_h values.

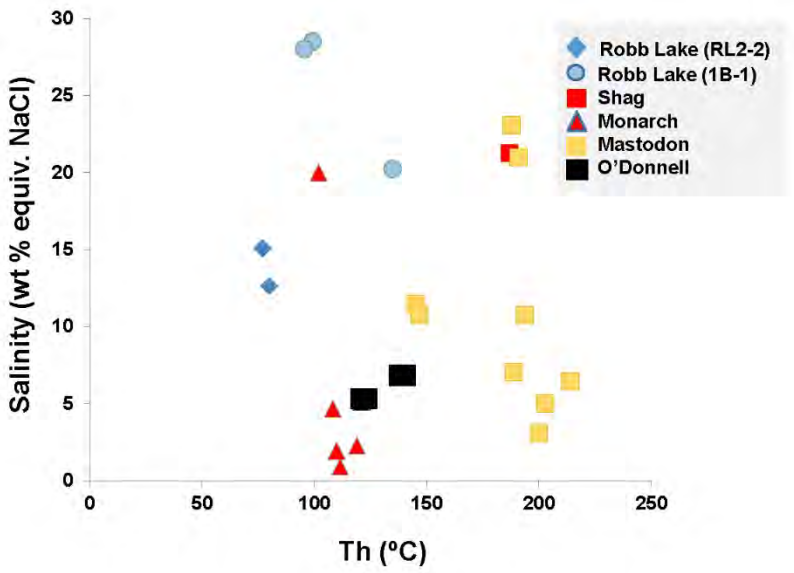

Figure 12: *Microthermometric data for sphalerite-hosted fluid inclusions plotted as homogenization temperature (Th) versus salinity (wt. % equiv. NaCl). Data are singular measurements except for Mastodon and Monarch, which are averages of a few fluid inclusions. Figure is from Kontak et al. (2022).*

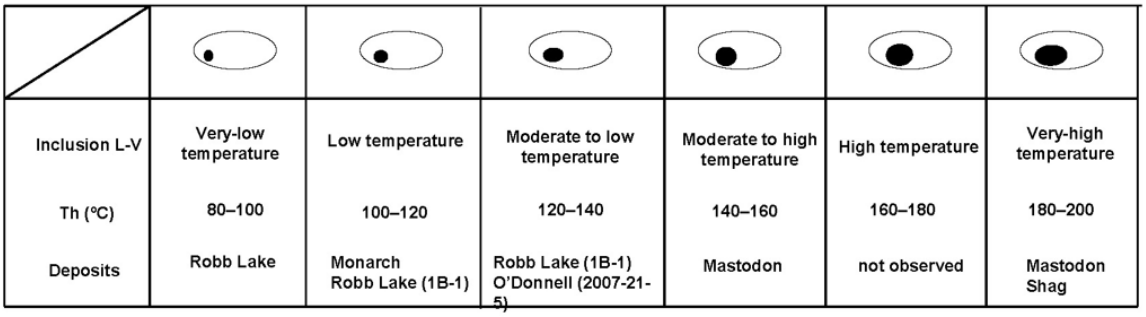

Inclusion L-V	Very-low temperature	Low temperature	Moderate to low temperature	Moderate to high temperature	High temperature	Very-high temperature
Th (°C)	80–100	100–120	120–140	140–160	160–180	180–200
Deposits	Robb Lake	Monarch Robb Lake (1B-1)	Robb Lake (1B-1) O'Donnell (2007-21-5)	Mastodon	not observed	Mastodon Shag

Figure 13: *Summary of schematic fluid inclusions with range of V-L ratios as observed in sphalerite from different mineralized settings. The estimated Th values shown are based on actual Th data and equate to what is inferred based on the temperature-density plot for the pure H_2O system (Roedder, 1984). This approach was used to infer Th values for sphalerite-hosted fluid inclusions as part of fluid inclusion assemblages in order to compare data across deposit settings. Note that none of the inclusions studied had V-L ratios indicative of Th = 160 to 180°C. Figure is from Kontak et al. (2022).*

Plotting the T_h and salinity data (Fig. 12) indicates a very broad inverse trend in which salinity decreases with increasing Th and that for any one site there can be a large range in these data. Additionally, that there is there is not a well-defined mixing trend involving two endmember fluids suggests instead the possible mixing of several fluids with varying salinity and temperature.

Secondary ion mass spectrometry (SIMS) isotopic (S, O) studies

For this study, in situ SIMS isotopic measurements were made versus conventional bulk analysis to track subtle changes that the latter method might not detect. The analysed points were selected based on petrographic study with data generated for carbonate and sulphide phases in close proximity (<1 cm). Data for 5 representative samples were obtained to cover the paragenetic context of carbonate and sulphide phases. In many cases multiple points were made on the same grain. Further details are provided in Kontak *et al.* (2022).

The results of $\delta^{34}S_{VCDT}$ are summarized below.

- For the Great Slave Reef area of the Pine Point district coarse-grained sphalerite intergrown with carbonate yielded values of 23.6 to 24.9‰
- For Reeves MacDonald of the Kootenay Arc district four sphalerite grains intergrown with matrix carbonate yielded values from 7.4 to 9.3‰.
- In the Rocky Mountains, four analyses of coarse yellow to reddish sphalerite from Robb Lake intergrown with carbonate minerals yielded values of 16.6 to

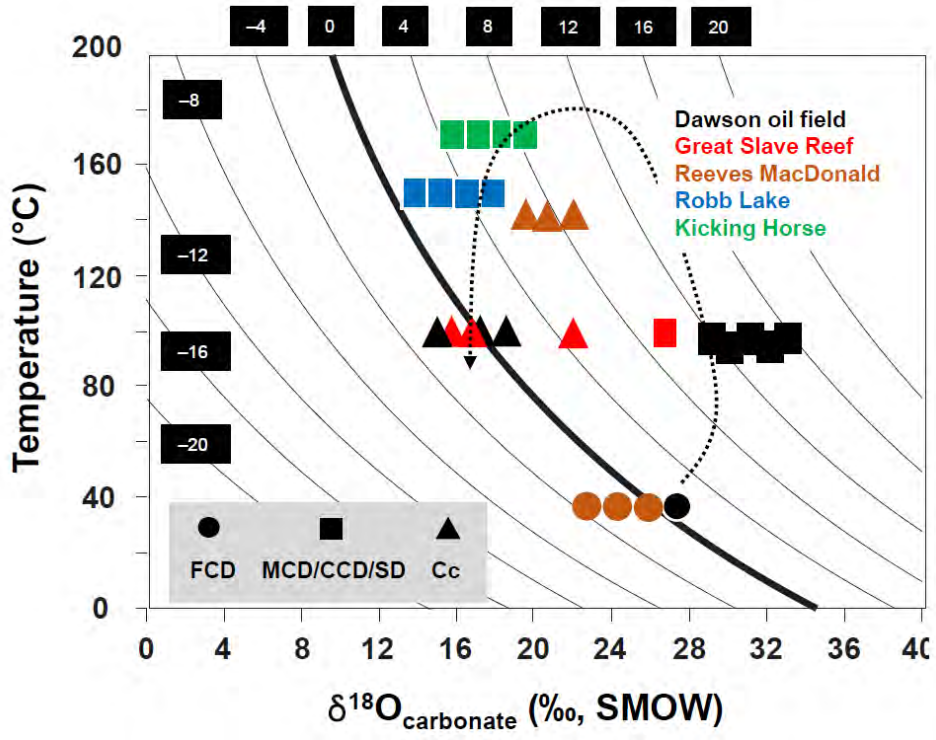

Figure 14: *Plot of $\delta^{18}O_{carbonate}$ (‰; VSMOW) values for various carbonate types versus estimated temperatures of formation, as discussed in text. Curved lines are isopleths of $\delta^{18}O_{H2O}$ values (indicated by the black boxes) of precipitating fluids calculated using the dolomite-H_2O fractionation equation (Horita, 2014). Note data are colour coded by setting and symbols denote carbonate type. As the in-situ SIMS data for each phase per sample analyzed was uniform (i.e. ±1–2‰), average values are plotted. Additionally, since the difference in the calcite-H_2O fractionation (compared to dolomite- H_2O) is not significant (i.e., 2‰ at 100°C; Horita, 2014), only the isopleths for dolomite- H_2O fractionation are shown. The dashed black line traces the idealized evolutionary trend of a fluid in a MVT-type setting. Abbreviations: Cc: calcite; CCD: coarse-grained crystalline dolomite; FCD: fine-grained crystalline dolostone; MCD: medium-grained crystalline dolomite; SD: saddle dolomite. Figure is from Kontak et al. (2022).*

19.3‰. In contrast, for Kicking Horse small euhedral pyrite grains (n = 6) yielded values from 29.3 to 31.4‰ and two sphalerite grains yielded similar values of 33.2‰ (n=2) and 29.4 to 31.6‰ (n=2).

The results of $\delta^{18}O_{VSMOW}$ for carbonate are summarized below.

- Data for the Dawson oil field yielded the following results: 1) pre-ore fine-grained crystalline dolostone (n=3) yielded similar values of 27.0 to 27.9‰; 2) syn-ore coarse-grained crystalline dolomite (n-=5) yielded values of 29.0 to 33.2‰; 3) post-ore coarse saddle dolomite (n=4) yielded values of 27.9 to 33.1‰; and 4) post-ore calcite (n=6) yielded values of 15.5 to 18.4‰.
- For the Great Slave Reef setting, pre-ore coarse-grained crystalline dolomite (n=4) yielded values of 26.1 to 27.3‰ (D3, D4), whereas for post-ore calcite 2 grains yielded values of 21.3 to 23.1‰ and 15.7 to 17.6‰.
- In the Kootenay Arc, data for Reeves MacDonald deposit include: 1) pre-ore fine-grained crystalline dolostone (n=3) with values of 22.2 to 26.0‰ (D1–D3) and 2) post-ore calcite (n=4) with values of 19.8 to 22.0‰.
- In the Rocky Mountains, data are for Robb Lake and Kicking Horse. At the former, early medium-grained crystalline dolomite and syn-ore coarse-grained crystalline dolomite yielded values of 13.4 and 16.7‰, whereas post-ore coarse saddle dolomite (n=4) yielded of 13.8 to 17.1‰. For Kicking Horse, pre-/syn-ore medium-grained crystalline dolomite (n=2) yielded values of 17.3 to 19.5‰, whereas coarse post-ore saddle dolomite (n=3) yielded values of 16.0 to 19.5‰.

Discussion

General deposit characteristics

This study used a similar classification for all ore and gangue phases as previous workers to facilitate comparison of both local and regional variability of deposit features using the above characteristics. The results of this comparison are summarized below.

The paragenesis for all sites indicates initial marine

cementation was followed by a widespread dolomitization related to the formation of specific textural types of dolomites, that is fine-grained crystalline through to saddle type. Importantly this aligns with previous studies (e.g., Qing 1991, 1998; Qing & Mountjoy, 1994; Nelson *et al.*, 2002; Paradis *et al*., 2006; Paradis & Simandl, 2019) despite age differences for host rocks and fluid flux flow. CL imaging of select samples reflects a textural modification accompanying diagenesis of the host rocks from an early fine-grained crystalline dolostone through to latter medium-grained and coarse-grained crystalline dolomite types and finally saddle dolomite. This observation of dolomite textural coarsening aligns with sulphide formation and signals its relevance in regard to the mineralizing event.

A simple sulphide mineralogy occurs and is dominated by sphalerite, galena, and pyrite; marcasite and chalcopyrite are rare. The sulphide precipitation commenced with an initial stage of these phases and was followed by the same mineral phases, albeit punctuated by some brecciation which is most apparent for the few samples studied from Pine Point. This later sulphide stage was accompanied by a second dolomitization event represented by coarse-grained varieties of dolomite that are syn- or post-sulphides. Commensurate with this is higher Fe contents of these latter dolomites, in addition to some having micro-inclusions of sphalerite (i.e., indicated by their anomalous Zn values (to 1.2 wt.% ZnO)

The deposition of the sulphides and gangue phases in MVT settings is complex and involves the interplay of many factors - host rock dissolution and replacement, fracturing and open space filling, sulphide formation, and brecciation - in addition to fluid mixing (Leach *et al*. 2005; Wilkinson, 2014). Evidence of breccias is noted for all settings and important for creating porosity and permeability for the ingressing fluids.

Sulphide textures vary, but here the focus is on sphalerite as it is the most important ore phase and as such provides insight to conditions attending mineralization. For example, well-developed banding in sphalerite (colloform texture), common at many sites, is variably interpreted in the literature (see reviews by Barrie *et al*. [2009] and Boyce *et al*. [2015]) as due to: 1) interplay among crystal growth, diffusion of solutes, and surface tension, which results in self-organized patterns (Fowler & Heureux, 1996). Fowler & Heureux (1996) attribute this to the alternating Fe and Zn contents at the micro-scale (0.1 to 1.0 mm), but Roedder (1968a) noted the lack of such a correlation in all samples at Pine Point ore; 2) colloidal suspension due to fluid mixing, such as in the Irish-type deposits (Barrie *et al*., 2009; Boyce *et al*., 2015); and 3) supersaturation due to fluid mixing versus colloid formation (Roedder, 1968b). Regardless, relevant for MVT ore system is the importance and strong evidence of colloform texture and fluid mixing (Leach *et al*., 2005, 2010b; Wilkinson, 2014). The latter is supported from both previous and our new FI studies documenting a range in fluid salinities (i.e., <1–30 wt. % equiv. NaCl), hence fluid mixing during sphalerite mineralization critical for development of colloform-banded ores. As for fluid sources in the study area, the lack of magmatic and metamorphic events overlapping mineralization precludes the role of such fluid sources, which leaves meteoric fluids and basinal-brines as candidate fluids, as discussed later.

Replacement textures are widespread in the studied samples, in particular related to the development of the various carbonate types – i.e., fine-grained crystalline dolostone through to the many coarser varieties – which is attributed to coupled dissolution and re-precipitation of carbonate minerals (e.g., Putnis, 2009). That sphalerite formation overlaps paragenetically with the medium- to coarse-grained crystalline dolomite phases likely indicates the mineralizing event was facilitated by generation of porosity due to dissolution of earlier carbonate minerals which is a self-sustaining process as sulphide formation is acid generating, such as recently discussed for SedEx-type mineralization by Magnall *et al.* (2022).

The commonly observed colour zonation in sphalerite (i.e., red-brown or light red-yellow to clearer sphalerite) may reflect a fluxing state of fluid chemistry (e.g.., fO_2, fS_2). However, sphalerite texture, regardless of colour, is highly variable from fine- to coarse-grained and disseminated to pervasive, and locally massive with nearly complete replacement of the host carbonates. That sulphide mineralization is locally selective is intriguing but was not a focus of follow-up studies. It is noted, however, that the presence of haloes of disseminated sphalerite around coarser sphalerite, as seen in CL images, reflects the micron-scale nature of the coupled dissolution, replacement and mineralizing process all acting in concert. Two options are considered for the latter observation: 1) an earlier sphalerite event commensurate with dolostone formation which thereby infers a protracted episode of Zn-mineralization; or 2) further ingress of fluids beyond where coarse sphalerite forms and thus related to formation of coarse crystalline dolomite phases and thus part of the main Zn-forming event, which is the favoured interpretation.

Lastly, we note the unusual occurrence of hopper and dendritic type galena at Pine Point. Such textures are attributed to rapid precipitation brought about by disequilibrium, such as fluid mixing. The latter is therefore consistent with a mixing model for this setting, which is discussed in more detail by Szmihelsky *et al.* (2020). It does, however, raise the question as to why such textures are not more common if this model is in fact valid for MVT settings (e.g., Leach *et al.*, 2005), although it has recently been reported by Mathieu *et al.* (2022) for settings in Arctic Canada.

Carbonate mineral chemistry

Five carbonate mineral phases were noted based on petrographic and chemical data and some of their features suggest growth during ingress of a mineralizing fluid. Thus, although early dolomites are mostly stoichiometric, some fine-grained crystalline types have <1.4 wt. % FeO related to a paragenetically later, Fe-rich fluid, which is supported by CL images showing traces of disseminated sphalerite. The Fe-rich saddle dolomite phase may also record a modified signature via interaction with a later fluid as also suggested from micro-inclusions of sphalerite, as indicated by elevated Zn contents (<1.2 wt. % ZnO, and CL images with sphalerite inclusions. The latest dolomite is the most Fe rich, having both a distinct chemistry and bright red CL signature. The latter features are attributed to two processes: 1) cessation of sphalerite formation; and 2) change in redox such that sulphate dominated over sulphide, which terminates precipitation of Fe-bearing sulphide

phases. Both processes would cause preferential enrichment of Fe in the saddle dolomite.

Fluid inclusions

The FIs in sphalerite provide insight into the thermal and chemical characteristics of the ore fluids regardless of their time of entrapment (i.e., primary through secondary types). A conclusion supported by the similarity of FIs data for various settings in the present study versus MVT districts in general (Basuki &Spooner, 2004; Bodnar *et al*., 2014; Wilkinson, 2014).

The T_h data, both measured and derived from V:L ratios, indicate lower T_h values (77 to 135°C) are mainly confined to the Rocky Mountain deposits (except for one Shag sample at 187°C) which conform to those generally reported for MVT deposits globally, as noted above. Assuming these fluids were in thermal equilibrium with their host rocks, then depths of formation are inferred to be between 2.0 to 4.0 km using a geotherm of 30°C. Additionally, assuming lithostatic conditions the pressure correction temperatures for 30 bar/°C (Steele-MacInnis *et al.*, 2012) vary between 100 and 180°C (for T_h of 77–135°C), which are maximum since a component of hydrostatic pressure is likely in these settings.

The higher T_h values of 145 to 214°C for the Mastodon samples of the Kootenay Arc are higher than the 121 to 140°C T_h values for the O'Donnell samples, also from the Kootenay Arc. For these, estimates of formation depths range from 5 to 7 km for parameters as above, with shallower depths if thermal equilibrium was not attained. Pressure corrected Th values, again as above, range between 195 and 280°C, thus well beyond that typical for MVT deposits (Leach *et al.*, 2005; Bodnar *et al*., 2014; Wilkinson, 2014). Again, as noted above, some hydrostatic component is likely. Finally, the unusually high T*h* values for the Kootenay Arc deposits are more similar to such data for Irish-type Zn-Pb deposits (e.g., Wilkinson, 2001, 2014) which suggests a high geothermal gradient. That some chalcopyrite mineralization is present in the Kootenay Arc samples is noted, which is consistent with the inferred higher formation temperatures.

The salinity data for sphalerite-hosted FIs ranges from <1 to 28 wt. % equiv. NaCl ($\pm CaCl_2$), but smaller for any single setting: Robb Lake: 10 to 28, Monarch less than 1 to 21, and Mastodon 5 to 23; both O'Donnell (5–7) and Shag (21–22) have very narrow ranges. For the latter, no earlier studies recorded salinities below 7 wt. % equiv. NaCl, but value of 1 wt. % equiv. NaCl were reported for post-ore calcite at Pine Point (Roedder, 1968c; Turner, 2006). As no data for sphalerite were recorded in this study for Pine Point, we cannot address the latter differences in salinity. We can however make a comparison for the Monarch setting where salinities recorded for sphalerite-hosted FIs are between 1 and 6 (n=6) and 20 (n=3) wt. % equiv. NaCl. These data contrast with data (n=23) in Vandeginste *et al*. (2007) that were >20 wt. % equiv. NaCl. These low-salinity values recorded for Monarch contrast with the generalization that MVT fluids are of high salinity; although low salinities may occur in gangue phases (Basuki & Spooner, 2004; Leach *et al.*, 2005; Bodnar *et al*., 2014).

Finally, in Th-salinity space (Fig. 12) the data show a general trend of lower salinity with increasing Th. Although more data are needed, these results can only be accommodated by a simple model that involves the dilution of a saline fluid by a less saline one. That some data (e.g., Monarch) fall below unmodified seawater (i.e., 3.2 wt. % NaCl; Bischoff & Rosenbauer, 1985), also implies involvement of meteoric water.

Isotopic data

Stable isotopes are used to trace the possible source reservoirs for metals and anions (e.g., S) and to assess processes (e.g., T, pH, or fO_2) in ore deposit formation (e.g., Ohmoto & Rye, 1979). This aspect explored below, but also in the context of the SIMS approach to such studies where high-resolution understanding of the paragenesis is needed, such as the different carbonate phases noted in this study.

Sulphur isotopes

The in situ $\delta^{34}S_{VCDT}$ data for single sphalerite grains from the 4 sites reveal uniform values: 1) 23.6 to 24.9‰ for Great Slave Reef, Pine Point district; 2) 8.4 to 9.3‰ for Reeves MacDonald, Kootenay Arc; and 3) 17.1 to 19.3‰ for Robb Lake and 29.4 to 33.2‰ for Kicking Horse in the Rocky Mountain fold and thrust belt; for the latter, pyrite yielded 29.3 to 31.4‰. For Kicking Horse, the Δpyrite-sphalerite of –1.4‰ differs from that predicted for formation at approximately 200°C (using FI data) which suggests a subtle change in some parameters when these phases grew and as such is an example of the usefulness of the high spatial resolution offered by SIMS.

That the $\delta^{34}S_{VCDT}$ for sulphides are generally uniform within single MVT settings (i.e., Δsulphide <5‰) large differences occur among different deposits (i.e., Δsulphide to >40‰; Ohmoto & Rye, 1979; Leach *et al.*, 2005). The latter reflects the different ways S can be reduced from its oxidized form, either thermochemical sulphate reduction (TSR) or bacterial sulphate reduction (BSR). Where TSR dominates, $\delta^{34}S_{VCD}$ values are either similar to the starting sulphate in the fluid or up to 10 to 15‰ less depending on total versus partial (i.e., distillation) reduction of the sulphate (e.g., Wilkinson, 2014; Brueckner *et al.*, 2015). In contrast, BSR generates much lower $\delta^{34}S_{VCD}$ values related to fractionation (i.e., 10s‰) via metabolism (Seal, 2006). Also relevant is the secular variability of $\delta^{34}S$ of evaporitic sulphate (Farquhar *et al.*, 2010).

Based on the above discussion, the $\delta^{34}S_{VCD}$ sphalerite data are therefore interpreted. For the Great Slave Reef ($\delta^{34}S_{VCD} \approx$ 25‰), which is similar to data for Pine Point orebodies (≈ 21‰; Sasaki and Krouse, 1969), and Kicking Horse ($\delta^{34}S_{VCD}$ also with pyrite ≈ 31‰), an evaporitic source coupled with an efficient TSR produced reduced S (i.e., H_2S). In contrast, at Reeves MacDonald (≈ 9‰), either partial TSR of sulphate occurred or mixing of TSR and BSR produced reduced S in adequate proportions Lastly, for Robb Lake (≈ 18‰), a partial TSR process (i.e., distillation with the proportion of sulphate reduced was (≈70–80%) is considered the likely means of generating reduced S (e.g., Brueckner *et al*., 2015).

Oxygen isotopes

The *in-situ* SIMS $\delta^{18}O_{VSMOW}$ data are used to track fluid evolution and fluid-rock interactions commencing with early marine cementation (i.e. fine-grained crystalline dolostone), through various coarser dolomites (medium-grained

crystalline dolomite, coarse-grained crystalline dolomite, and saddle dolomite) and latest calcite occluding cavities. To account for the temperature dependent ^{18}O fractionation between carbonate minerals and fluid (Ohmoto, 1986), this was constrained using FIs data from both our study and earlier work for the relevant material, as discussed in Kontak *et al*. (2022).

Using these temperature constraints and the $\delta^{18}O_{VSMOW}$ carbonate data, a plot of temperature (°C) versus $\delta^{18}O_{carbonate}$ was constructed with isopleths for $\delta^{18}O_{H2O}$ (Fig. 14). The earliest stage of dolomite formation is represented by dolostone from the Dawson oil field and Reeves MacDonald, which either retained an original marine signature or reflects equilibration with seawater at low temperature. This is followed by growth of coarse dolomite phases having much lower $\delta^{18}O$ values due to its interaction with warm fluids having variable $\delta^{18}O_{H2O}$ signatures of 4 to 16‰ that are typical of basinal-type fluids (e.g., Wilkinson, 2014) and considered to best approximate the $\delta^{18}O_{H2O}$ of the Zn-Pb mineralizing fluids. Importantly, the variable $\delta^{18}O$ values are attributed to different fluid-rock ratios such that values furthest from those of the host dolostone reflect equilibration with the fluid (i.e., highest fluid-rock ratios). In this context, the data can be arranged to reflect the highest to lowest fluid-rock ratio (Fig. 14): Dawson oil field, Kicking Horse, and Robb Lake. Additionally, it should be noted that in this conclusion is highly subject to changing temperature with the greatest effect at lower (i.e., <100°C) versus higher temperatures due to greater dependence on calculated $\delta^{18}O_{H2O}$ values (see change in slopes of isopleths in Fig. 14). Lastly is late-stage calcite that represents a much later fluid event. Notably the calcite data for Reeves MacDonald has the highest inferred $\delta^{18}O_{H2O}$ values (6–12‰), which may reflect a greater host rock influence whereas for Great Slave Reef and Dawson oil field the more depleted $\delta^{18}O_{H2O}$ data may reflect a more fluid-dominated system.

In summary, the $\delta^{18}O$ data reflect an early marine dolomitization (i.e., fine-grained dolostone) in the presence of a seawater-dominated fluid ($\delta^{18}O_{H2O} \approx 0$‰) followed by growth of coarser dolomite types via CDP processes related to ingress of heated fluids with elevated $\delta^{18}O_{H2O}$ values ($\delta^{18}O_{H2O} \approx$ 4-16‰) commensurate with burial and, lastly, post-ore calcite which records again the involvement of surficial fluids, in this case meteoric ($\delta^{18}O_{H2O} \approx 0$‰). Importantly, these conclusions reflect our integration of petrography and paragenesis with in situ SIMS data and accounts for the interaction of rock and fluid which is now seen as replacement, via CDP processes, of early fine-grained crystalline dolostone by later coarser crystalline and saddle dolomites. The variation of $\delta^{18}O$ data for such settings can be accounted for in the context (i.e., fluid:rock ratio) and is not simply a function of fluid temperature. This conclusion is relevant as it suggests that the most abundant and highest-grade mineralization is expected where at sites of greatest fluid-rock interaction as the ore system equilibrates toward the ingressing mineralizing fluid, as suggested for both MVT settings (Savard *et al*., 2000) and Carlin-type gold deposits (Barker *et al.*, 2013).

Summary and Conclusions

A detailed petrographic, geochemical (SEM-EDS, CL), and in situ SIMS isotopic (O, S) study of a suite of samples from three MVT districts across the eastern Canadian Cordillera represents the first geographically comprehensive examination of such materials as part of a single study. It provides, therefore, the means to compare and contrast materials and evaluate derived observations and data.

In all three districts, a similar paragenesis in noted and concurs with earlier studies. It involved initial widespread dolomitization of marine carbonate rocks followed by different stages of hydrothermal dolomite formation (e.g., medium- to coarse-grained crystalline and saddle dolomites) and sulphide deposition of mainly sphalerite with additional galena and pyrite with later cavity- and fracture-filling carbonate minerals. The sphalerite is divided into two stages – an early light to dark red-brown transitioning to a later pale, honey-yellow type; it also occurs as a later stage colloform or banded textured variety where it occludes open space. Galena is paragenetically later with rare hopper or dendritic morphology indicative rapid growth.

Conditions attending ore formation were constrained via sphalerite-hosted FIs. Thus, for the Rocky Mountain fold and thrust belt trapping temperatures of 100–180°C are noted versus 195–280°C for the Kootenay Arc. Salinities of mineralizing fluids are varied (1 to 28 wt. % equiv. NaCl (±CaCl2)), but with narrower ranges for single settings. This T-salinity variation among MVT districts implicates different fluid reservoirs, which best equate to basinal-type fluids and surficial or meteoric fluids. The presence of bitumen was rarely noted except for the Great Slave Lake, Pine Point district (Western Canadian Sedimentary Basin) and Munroe and Shag (Rocky Mountains) indicating that locally liquid petroleum flowed through these systems synchronous with ore formation. As suggested by Szmihelsky *et al*. (2020), this likely triggered some of the sphalerite formation at Pine Point.

Four distinct textural varieties of dolomite of similar paragenesis were identified in all the MVT districts studied. Early fine-grained and medium-grained crystalline dolomite are generally Fe poor, but the later coarser grained dolomite contains Fe and (locally) Zn (as micro-inclusions of sphalerite) and thus consistent with this later coarser grained dolomite overlapping mineralization. Saddle dolomite, which is the most Fe rich, is syn- to post-sphalerite and the latest dolomite to precipitate. CL observations indicate the imprint of the Zn (±Pb) mineralizing fluid was more pervasive than petrographic observations suggest and thus this tool should be more integrated into studies. In general, therefore, results suggest the paragenesis and fluid (migration) histories in the studied MVT systems may (in some deposits or districts) be more complex than previously considered.

In situ $\delta^{34}S_{VCDT}$ (sphalerite, pyrite) and $\delta^{18}O_{VSMOW}$ (carbonate minerals) data were used to assess the use of this method versus conventional bulk-type analysis done previously. As results are comparable to previous data, where available, isotopic homogeneity at a micron scale is inferred. The $\delta^{34}S_{VCDT}$ data agree with earlier conclusions invoking an evaporitic source for sulphur with TSR the dominant processes to generate the reduced S in the precipitated sulphides. Possible contribution of reduced SA via BSR processes is noted for only one site (i.e., Reeves MacDonald). That TSR was the dominant process that generated reduced S species (i.e., H_2S) species suggests a H_2S -bearing fluid was likely at the sites of mineralization prior to ingress of the metal-bearing fluid, or fluid-flow paths intersected there. The $\delta^{18}O_{VSMOW}$ data reflect evolution of fluid-

rock interactions that account for the sequential formation of the carbonate types during burial and mineralization. The documented signatures of these carbonate phases reflect variable rock and $\delta^{18}O_{H2O}$ values (i.e., reservoirs), changing thermal conditions, and different fluid-rock ratios.

Collectively, the data sets suggest at least three fluids are responsible for the documented chemical signature of the mineralized sites: FI studies require at least two (if not more) fluid reservoirs whereas the $\delta^{34}S_{VCDT}$ data indicate TSR was the dominant process to generate reduced sulphide, which indicates that metals were transported by another fluid poor in sulphur. As with previous models for MVT deposits (Leach *et al*., 2005, 2010a, b; Wilkinson, 2014), a two-fluid mixing model is favoured as TSR is a relatively slow process, thus, the most efficient ore-formation process is to have a ready supply of sulphur where mineralization is formed (also see recent discussion in Mathieu *et al.*, 2022). The two-fluid mixing model is also favoured by the presence of colloform-textured sphalerite at many of the study sites, but in particular at Pine Point (see discussion in Szmihelsky *et al*. (2020). Lastly, the $\delta^{18}O_{VSMOW}$ data are consistent with multiple fluid reservoirs, including a surficial or meteoric water fluid reservoir.

Acknowledgements

This paper is derived from an earlier paper that formed a contribution to Natural Resource Canada's Targeted Geoscience Initiative program (TGI-5). and, as such, benefited from financial support through the Volcanic- and Sedimentary-hosted Base Metal Mineralization project's 'Activity VS-2.1: Is there a genetic link between various types of sediment-hosted deposits of the Canadian Cordillera?'. The earlier paper benefited from critical reviews by Drs. J. Peter, M. Gadd, and G. Chi that the authors sincerely appreciated. We thank Dr. Colin Andrew for the invite to contribute to this special volume.

Source of Funding

This data acquired and presented in this paper was made possible from Natural Resources Canada via their Targeted Geoscience Initiative program (TGI-5) under the Volcanic- and Sedimentary-hosted Base Metal Mineralization project's 'Activity VS-2.1: Is there a genetic link between various types of sediment-hosted deposits of the Canadian Cordillera?

References

Adams, J.J., Rostron, B.J., & Mendoza, C.A., (2000) Evidence for two-fluid mixing at Pine Point, NWT; *Journal of Geochemical Exploration*, v. 69–70, p. 103–108.

Atkinson, N. & Lyster, S., (2000) Thickness of Quaternary and Neogene sediment in Alberta, Canada; Energy Resources Conservation Board, ERCB/AGS MAP 551, scale 1:1 500 000.

Barker, S.L.L, Dipple, E.G.M., Hickey, K.A., Lepore, W.A., & Vaughn, V., (2013) Applying stable isotopes to mineral exploration: teaching an old dog new tricks; *Economic Geology*, v. 108, no. 1, p. 1–9.

Barrie, C.D., Boyce, A.J., Boyle, A.P., Williams, P.J., Blake, K., Lowther, J.M., McDermott, P., Wilkinson, J.J., & Prior, D.J., (2009) On the growth of colloform textures: a case study of sphalerite from the Galmoy ore body, Ireland; *Geological Society of London, Journal*, v. 166, no. 3, p. 463–483.

Basuki, N.I. & Spooner, E.T.C., (2004) A review of fluid inclusion temperatures and salinities in Mississippi Valley-type Zn-Pb deposits: identifying thresholds for metal transport; *Exploration and Mining Geology*, v. 11, no. 1–4, p. 1−17.

Bodnar, R.J., (2003) Re-equilibration of fluid inclusions; in Fluid inclusions: analysis and interpretation, (ed.) I.M. Samson, A.J. Anderson, and D. Marshall; *Mineralogical Association of Canada, Short Course Series*, v. 32, p. 213–230.

Bodnar, R.J., Reynolds, T.J., and Kuehn, C.A., (1985) Fluid-inclusion systematics in epithermal systems; Reviews in Economic Geology, v. 2, p. 73–97.

Bodnar, R.J., (2003a) Introduction to fluid inclusions; in Fluid inclusions: analysis and interpretation, (ed.) I.M. Samson, A.J. Anderson, and D. Marshall; *Mineralogical Association of Canada, Short Course Series*, v. 32, p. 1–8.

Bodnar, R.J., (2003b) Re-equilibration of fluid inclusions; in Fluid inclusions: analysis and interpretation, (ed.) I.M. Samson, A.J. Anderson, and D. Marshall; *Mineralogical Association of Canada, Short Course Series*, v. 32, p. 213–230.

Bodnar, R.J., Lecumberri-Sanchez, P., Moncada, D., & Steele-MacInnis, M., (2014) Fluid inclusions in hydrothermal ore deposits; Chapter 5 in Vol. 13: Geochemistry of mineral deposits; Treatise on geochemistry, 2nd edition, (ed.) S.D. Scott; Elsevier, Oxford, United Kingdom, p. 119–142.

Boyce, A.J., Barrie, C.D., Samson, I.M., & Williams-Jones, A.E., (2015) Aspects of the geochemistry of zinc – a journey to sphalerite; in Current perspectives on zinc deposits, (ed.) S.M. Archibald and S.J. Piercey; *Irish Association for Economic Geology, Dublin, Ireland*, p. 17–35.

Bischoff, J.L., & Rosenbauer, R.J., (1985) An empirical equation of state for hydrothermal seawater (3.2 percent NaCl); *American Journal of Science*, v. 285, no. 8, p. 725–763.

Brueckner, S.M., Piercey, S.J., Layne, G.D., Piercey, G., & Sylvester, P.J., (2015) Variations of sulphur isotope signatures in sulfides from the metamorphosed Ming Cu(−Au) volcanogenic massive sulphide deposit, Newfoundland Appalachians, Canada; *Mineralium Deposita*, v. 50, p. 619–640.

Drage, N. & Paradis, S., (2018) Geology and petrography of selected carbonate-hosted Zn-Pb deposits of the southeastern Cordillera, British Columbia and Alberta; *Geological Survey of Canada*, Open File 8410, 27 p.

Farquhar, J., Wu, N.P., Canfield, D.E., & Oduro, H., (2010) Connections between sulphur cycle evolution, suphur isotopes, sediments, and base metal VMS, SEDEX, and MVT deposits; *Economic Geology*, v. 105, p. 509–533.

Fowler, A., & L'Heureux, I., (1996) Self-organized banded sphalerite and branching galena in the Pine Point ore deposit, Northwest Territories; *The Canadian Mineralogist*, v. 34, no. 6, p. 1211–1222.

Götze, J., (2012) Application of cathodoluminescence microscopy and spectroscopy in geosciences; *Microscopy and Microanalysis*, v. 18, p. 1270–1284.

Götze, J., Hans-Peter Schertl, H.-P., Neuser, R.D., Kempe, U., & Hanchar, H.M., (2013) Optical microscope-cathodoluminescence (OM–CL) imaging as a powerful tool to reveal internal textures of minerals; *Mineralogy and Petrology*, v. 107, p. 373–392.

Goldstein, R.H. & Reynolds, T.J., (1994) Systematics of fluid inclusions in diagenetic minerals; *Society for Sedimentary Geology, Short Course* No. 31, 199 p.

Hahn, K.E., Turner, E.C., Kontak, D.J., & Fayek, M., (2018) Fluid-chemical evidence for one billion years of fluid flow through Mesoproterozoic deep-water carbonate mounds (Nanisivik zinc district, Nunavut); *Geochimica et Cosmochimica Acta*, v. 223, p. 493–519.

Hannigan, P.K., (2006) Synthesis of Mississippi Valley-type lead-zinc deposit potential in northern Alberta and southern Northwest

Territories; in Potential for carbonate-hosted lead-zinc Mississippi Valley-type mineralization in northern Alberta and southern Northwest Territories: Geoscience Contributions, Targeted Geoscience Initiative, (ed.) P.K. Hannigan; *Geological Survey of Canada, Bulletin* 591, p. 305–347.

Horita, J., (2014) Oxygen and carbon isotope fractionation in the system dolomite-water-CO_2 to elevated temperatures; *Geochimica et Cosmochimica Acta*, v. 129, p. 111–124.

Höy, T., (1982) Stratigraphic and structural setting of stratabound lead-zinc deposits in southeastern British Columbia; *CIM Bulletin*, v. 75, p. 114–134.

Kontak, D.J, Paradis, S., Waller, Z., & Fayek, M., (2022) Petrographic, fluid inclusion and ion mass spectrometry stable isotopic (O, S) study of Mississippi Valley-type mineralization in British Columbia and Alberta. In: Targeted Geoscience Initiative 5: Volcanic- and sediment-hosted massive sulfide deposit genesis and exploration methods, (Ed.) J.M. Peter and M.G. Gadd; *Geol. Surv. Can*., Bulletin 617, 203-245.

Klyukin, Y.L., Steele-MacInnis, M., Lecumberri-Sancheza, P., & Bodnar, R.J. (2019) Fluid inclusion phase ratios, compositions and densities from ambient temperature to homogenization, based on PVTX properties of H_2O-NaCl; *Earth-Science Reviews*, v. 198, 102924.

Krebs, W.,& Macqueen, R., (1984) Sequence of diagenetic and mineralization events, Pine Point lead-zinc property, Northwest Territories; Canada; *Bulletin of Canadian Petroleum Geology*, v. 32, p. 434–464.

Kyle, J.R., (1981) Geology of the Pine Point lead–zinc district; Chapter 11 in Volume 9, Regional and specific deposits, 1st edition; Handbook of strata-bound and stratiform ore deposits, (ed.) K.H. Wolf; Elsevier, New York, U.S.A., v. 9, p. 643–741.

Leach, D.L., & Sangster, D.F., (1993) Mississippi Valley-type lead-zinc deposits; in Mineral deposit modelling, (ed.) R.V. Kirkham; Geological Association of Canada, Special Paper 40, p. 289–314.

Leach, D.L., Sangster, D.F., Kelley, K.D., Large, R.R., Garven, G., Allen, C.R., Gutzmer, J., & Walters, S., (2005) Sediment-hosted lead-zinc deposits: a global perspective; in Economic Geology, 100th anniversary volume, 1905–2005, (ed.) J.W. Hedenquist, J.F.H. Thompson, R.J. Goldfarb, and J.P. Richards; *Society of Economic Geologists*, Littleton, Colorado, p. 561–607.

Leach, D.L., Bradley, D.C., Huston, D., Pisarevsky, S.P., Taylor, R.D., & Garoll, S.J., (2010a) Sediment-hosted lead-zinc deposits in Earth history; *Economic Geology*, v. 105, no. 3, p. 593–625.

Leach, D.L., Taylor, R.D., Fey, D.L., Diehl, S.F., & Saltus, R.W., (2010b) A deposit model for Mississippi Valley-Type lead-zinc ores. Chapter A of Mineral Deposit Models for Resource Assessment; *U.S. Geological Survey Scientific Investigations Report* 2010–5070–A, 52 p.

Macqueen, R.W. & Thompson, R.I., (1978) Carbonate-hosted zinc-lead occurrences in northeastern British Columbia with emphasis on the Robb Lake deposit; Canadian Journal of Earth Sciences, v. 15, no. 11, p. 1737–1762.

Magnall, J., Wirth, R., Hayward, N., Gleeson, S.A., & Schreiber, A., (2022) Stratiform host-rock replacement via self-sustaining reactions in a clastic-dominated (CD-type) Zn deposit. *Economic Geology*, v. 118, no. 4, p. 823–836.

Mathieu, J., Turner, E.C., Kontak, D.J., Fayek, M., & Layne, G., (2015) In situ SIMS (O, S) and LA ICP-MS (trace elements) microanalysis of multiple cement phases reveal a complex diagenetic fluid history: A case study of Phanerozoic cements on Victoria Island, NWT; Chemical Geology, v. 415, p. 47–69.

Mathieu, J., Turner, E.C., Kontak, D.J., & Fayek, M., (2022) Geochemical evidence for a topographically driven regional mineralizing fluid in the Polaris Zn district, Arctic Canada. Economic Geology, v. 117, p. 1451–1480.

Meyers, W.J., (1974) Carbonate cement stratigraphy of the Lake Valley Formation (Mississippian) Sacramento Mountains, New Mexico; Journal of Sedimentary Research, v. 44, no. 3, p. 837–861.

McLemore, V.T. & Barker, J.M., (1987) Some geological application of cathodoluminescence: examples from the Lemitar Mountains and Riley travertine, Socorro County, New Mexico; *New Mexico Geology*, v. 15, p. 37–40.

McMechan, M.E., (2012) Deep transverse basement structural control of mineral systems in the southeastern Canadian Cordillera; *Canadian Journal of Earth Sciences*, v. 49, p. 693–708.

Moncada, D., Mutchler, S., Nieto, A., Reynolds, T.J., Rimstidt, J.D.,& Bodnar, R.J., (2012) Mineral textures and fluid inclusion petrography of the epithermal Ag–Au deposits at Guanajuato, Mexico: application to exploration; *Journal of Geochemical Exploration*, v. 114, p. 20–35.

Nelson, J., Paradis, S., Christensen, J., & Gabites, J., (2002) Canadian Cordilleran Mississippi Valley-type deposits: A case for Devonian-Mississippian back-arc hydrothermal origin; *Economic Geology*, v. 97, p. 1013–1036.

O'Connell, S., Dix, G.R., & Barclay, J.E., (1990) The origin, history, and regional structural development of the Peace River Arch, Western Canada; *Bulletin of Canadian Petroleum Geology*, v. 38A, p. 4–24.

Ohmoto, H., (1986) Stable isotope geochemistry of ore deposits; in Stable isotopes in high-temperature geological processes, (ed.) J.W. Valley, H.P. Taylor, Jr., and J.R. O'Neil; Mineralogical Association of America, *Reviews in Mineralogy*, v. 16, p. 185–225.

Ohmoto, H., & Rye, R.O., (1979) Isotopes of sulphur and carbon; in Geochemistry of hydrothermal ore deposits, 2nd edition, (ed.) H. Barnes; John Wiley and Sons, New York, p. 509–567.

Pană, D., (2006) Unravelling the structural control of Mississippi Valley-type deposits and prospects in carbonate sequences of the Western Canada Sedimentary Basin; in Potential for carbonate-hosted lead-zinc Mississippi Valley-type Mineralization in northern Alberta and southern Northwest Territories: geoscience contributions, Targeted Geoscience Initiative, (ed.) P.K. Hannigan; *Geological Survey of Canada, Bulletin* 591, p. 255–304.

Paradis, S., (2007) Carbonate-hosted Zn-Pb deposits in southern British Columbia: potential for Irish-type deposits; *Geological Survey of Canada, Current Research* 2007-A10, 10 p.

Paradis, S. & Nelson, J.L., (2007) Metallogeny of the Robb Lake carbonate-hosted zinc-lead district, northeastern British Columbia; in Mineral deposits of Canada: a synthesis of major deposit types, district metallogeny, the evolution of geological provinces, and exploration methods, (ed.) W.D. Goodfellow; *Geological Association of Canada, Mineral Deposits Division*, Special Publication No. 5, p. 633–654.

Paradis, S. & Simandl, G.J., (2017) Is there a genetic link between the SEDEX and MVT deposits of the Canadian Cordillera?; in Targeted Geoscience Initiative: 2016 report of activities, (ed.) N. Rogers; *Geological Survey of Canada*, Open File 8199, p. 107–113.

Paradis, S. & Simandl, G.J., (2019) Preliminary carbon and oxygen isotope analyses of hydrothermal carbonate from Mississippi Valley-type and REE-F-Ba deposits of the southern Canadian Rocky Mountains – a comparison; in Targeted Geoscience Initiative: 2018 report of activities, (ed.) N. Rogers; Geological Survey of Canada, Open File 8549, p. 205–216.

Paradis, S., Nelson, J.L., & Zantvoort, W., (1999) A new look at the Robb Lake carbonate-hosted lead-zinc deposit, northeastern British Columbia; *Geological Survey of Canada*, Current Research 1999-A, p. 61–70.

Paradis, S., Turner, W.A., Coniglio, M., Wilson, N., & Nelson, J.L., (2006) Stable and radiogenic isotopic signatures of mineralized Devonian carbonate rocks of the northern Rocky Mountains and the Western Canada Sedimentary Basin; in Potential for carbonate-hosted lead-zinc Mississippi Valley-type mineralization in northern Alberta and southern Northwest Territories: geoscience contributions, Targeted

Geoscience Initiative, (ed.) P.K. Hanningan;, *Geological Survey of Canada, Bulletin* 591, p. 75–103.

Paradis, S., Hannigan, P., & Dewing, K., 2007, Mississippi Valley-type lead-zinc deposits; in Mineral deposits of Canada: a synthesis of major deposit types, district metallogeny, the evolution of geological provinces, and exploration methods, (ed.) W.D. Goodfellow; *Geological Association of Canada, Mineral Deposits Division, Special Publicatio*n No. 5, p. 185–203.

Paradis, S., Keevil, H., Simandl, G.J., & Raudsepp, M., (2015) Carbonate-hosted nonsulphide Zn–Pb mineralization of southern British Columbia, Canada; *Mineralium Deposita*, v. 50, p. 923–951.

Paradis, S., Simandl, G.J., Drage, N., D'Souza, R.J., Kontak, D.J., & Waller, Z., (2022) Carbonate-hosted deposits (Mississippi Valley–type, magnesite, and REE-F-Ba) of the southeastern Canadian Cordillera: a review and isotopic data comparison; in Targeted Geoscience Initiative 5: Volcanic- and sediment-hosted massive sulfide deposit genesis and exploration methods, (ed.) J.M. Peter and M.G. Gadd; *Geological Survey of Canada, Bulletin* 118, no. 4, p. 823–836,

Paradis, S., Petts, D., Simandl, G.J., Sharpe, R., Hamilton, T.S., Fayek, M., & Jackson, S.E., (2023) Impact of deformation and metamorphism on sphalerite chemistry – element mapping of sphalerite in carbonate-hosted Zn-Pb sulfide deposits of the Kootenay Arc, southern British Columbia, Canada and northeastern Washington, USA. *Ore Geology Reviews*, v. 158,

Price, R.A., (1981) The Cordilleran foreland thrust and fold belt in the southern Canadian Rocky Mountains; in Thrust and nappe tectonics, (ed.) K.R. McClay and N.J. Price; *Geological Society of London, Special Publication* No. 9, p. 427–448.

Price, R A., (1994) Cordilleran tectonics and the evolution of the Western Canada Cordilleran Tectonics and the Evolution of the Western Canada Sedimentary Basin; in Geological Atlas of the Western Canada Sedimentary Basin; (comp.) G.D. Mossop and I. Shetson; Canadian Society of Petroleum Geologists and Alberta Research Council, Calgary, p. 13–24.

Putnis, A., (2009) Mineral replacement reactions; in Thermodynamics and Kinetics of Water-Rock Interaction, (ed) E.H. Oelkers and J. Schott; Mineralogical Society of America, *Reviews in Mineralogy and Geochemistry*, v. 70, p. 87–124.

Qing, H., (1991) Diagenesis of Middle Devonian Presqu'ile dolomite Pine Point NWT and adjacent subsurface; PhD thesis, McGill University, Montreal, P.Q., 292 p.

Qing, H., (1998) Petrography and geochemistry of early-stage, fine- and medium-crystalline dolomites in the Middle Devonian Presqu'ile Barrier at Pine Point, Canada; *Sedimentology*, v. 45, no. 2, p. 433–446.

Qing, H. & Mountjoy, E.W., (1992) Large-scale fluid flow in the Middle Devonian Presqu'ile barrier, Western Canada Sedimentary Basin; *Geology*, v. 20, no. 10, p. 903–906.

Qing, H. & Mountjoy, E.W., (1994) Origin of dissolution vugs, caverns, and breccias in the Middle Devonian Presqu'ile barrier, host of Pine Point Mississippi Valley-type deposits; *Economic Geology*, v. 89, no.4, p. 858–876.

Roedder, E., (1968a) Non-colloidal origin of colloform textures in sphalerite ores; *Economic Geology*, v. 63, no. 5, p. 451–471.

Roedder, R., (1968b) Sphalerite color banding: Lack of correlation with iron content, Pine Point, Northwest Territories, Canada; *American Mineralogist*, v. 53, no. 9–10, p. 1523–1529.

Roedder, E., (1968c) Temperature, salinity, and origin of the ore-forming fluids at Pine Point, Northwest Territories, Canada, from fluid inclusion studies; *Economic Geology*, v. 63, no. 5, p. 439-450.

Roedder, E., (1984) Fluid inclusions; in Reviews in mineralogy, (ed.) P.H. Ribbe; *Mineralogical Society of America*, v. 12, 644 p.

Sasaki, A., & Krouse, H.R., (1969) Sulphur isotopes and the Pine Point lead-zinc mineralization; *Economic Geology*, v. 64, p. 718–730.

Sangster, D.F. & Carrière, J.J., (1991) Preliminary studies of fluid inclusions in sphalerite from the Robb Lake Mississippi Valley-type deposit, British Columbia; *Geological Survey of Canada, Current Research* Part E, Paper No. 91-1E, p. 25–32.

Seal, R., (2006) Sulphur isotope geochemistry of sulfide minerals; in Sulfide Mineralogy and Geochemistry, (ed.) D.J. Vaughan; Mineralogical Society of America, *Reviews in Mineralogy and Geochemistry*, v. 61, p. 633–677.

Simandl, G.J., D'Souza, R.J., Paradis, S., & Spence, J., (2022) REE content of carbonate minerals in sediment-hosted Pb-Zn deposits, Canadian southern Rocky Mountains; in Targeted Geoscience Initiative 5: Volcanic- and sediment-hosted massive sulfide deposit genesis and exploration methods, (ed.) J.M. Peter and M.G. Gadd; Geological Survey of Canada, Bulletin 617, 165-201.

Szmihelsky, M., Steele-MacInnis, M., Bain, W.M., Falck, H., Adair, R., Campbell, R., Dufrane, S.A., Went, A., & Corlett, J.L., (2021) Mixing of brine with oil triggered sphalerite deposition at Pine Point, Northwest Territories, Canada. *Geology*, v. 49,

Steele-MacInnis, M., Lecumberri-Sanchez, P., & Bodnar, R.J., 2012, HOKIEFLINCS_H2O-NACL: A Microsoft Excel spreadsheet for interpreting microthermometric data from fluid inclusions based on the PVTX properties of H2O-NaCl; *Computer Geoscience*, v. 49, p. 334–337.

Turner, W. A., (2006) Microthermometric study of fluids associated with Pb–Zn mineralization in the vicinity of the Pine Point mining camp; in Potential for carbonate-hosted lead-zinc Mississippi Valley-type mineralization in northern Alberta and southern Northwest Territories: Geoscience Contributions, Targeted Geoscience Initiative, (ed.) P.K. Hannigan; *Geological Survey of Canada, Bulletin* 591, p. 221–240.

Vandeginste, V., Swennen, R., Gleeson, S.A., Ellam, R.M., Osadetz, K., & Roure, F., (2007) Geochemical constraints on the origin of the Kicking Horse and Monarch Mississippi Valley-type lead-zinc ore deposits, southeast British Columbia, Canada; *Mineralium Deposita*, v. 42, no. 8, p. 913–935.

Wilkinson, J.J., 2014, Sediment-hosted zinc-lead mineralization: processes and perspectives; in Geochemistry of mineral deposits: Treatise on geochemistry (second edition), (ed.) S.D. Scott; Elsevier, v. 13, p. 219–249.

Wilkinson, J.J., (2017) Metastable freezing: A new method for the estimation of salinity in aqueous fluid inclusions; *Economic Geology*, v. 112, no. 1, p. 185–193.